universe

MDPI

Article

TD-DFT Investigation of Sulfur and Chlorine Species as Potential Contributors to Venusian Unknown UV Absorber

Parmanand Pandey [1,2], Pravi Mishra [1,2], Rachana Singh [1,2], Manisha Yadav [2], Shivani [2], Aftab Ahamad [2], Alka Misra [1,*], Poonam Tandon [2] and Amritanshu Shukla [2,*]

[1] Department of Mathematics and Astronomy, University of Lucknow, Lucknow 226007, India; parmanand.physics@gmail.com (P.P.); pravimishra231@gmail.com (P.M.); singh.rchncat@gmail.com (R.S.)
[2] Department of Physics, University of Lucknow, Lucknow 226007, India; yadavmanisha605@gmail.com (M.Y.); physics.shiv@gmail.com (S.); aftabhmd710@gmail.com (A.A.); tandon_poonam@lkouniv.ac.in (P.T.)
* Correspondence: alkamisra99@gmail.com (A.M.); amritanshushukla@gmail.com (A.S.); Tel.: +91-9305666576 or +91-9415580700 (A.M.)

Abstract

The identification of the chemical species responsible for the anomalous near-ultraviolet (UV) opacity in the Venusian cloud for "unknown absorber" remains a paramount challenge in planetary science. This study presents a comprehensive quantum chemical investigation into a broad suite of candidate molecules, including isomers of thiosulfeno (S_2O_2), the hydroxysulfonyl radical (HSO_3), disulfur monoxide (S_2O), disulfur dichloride (S_2Cl_2), iron(III) chloride ($FeCl_3$), phosphine (PH_3), and structural isomers of polysulfur oxides (S_3O). Utilizing Time-Dependent Density Functional Theory (TD-DFT) at the CAM-B3LYP/def2-TZVPP level of theory, we systematically mapped electronic transitions across three distinct environmental phases: gas-phase (without solvent), supercritical CO_2, and concentrated H_2SO_4 aerosols. To establish confidence in the predicted results, our TD-DFT approach was rigorously benchmarked against high-level theoretical methods (CCSD(T), EOM-CCSD, and MRCI+Q) from recent literature. All these electronic transitions were modeled via the Solvation Model based on Density (SMD). Our results demonstrate a profound topological and environmental dependence on spectral signatures. Among the candidates, trans-OSSO (t-OSSO) emerged as the most viable near-UV absorber candidate, exhibiting a highly allowed $\pi \rightarrow \pi^*$ transition at 379.37 nm (f = 0.1140) in H_2SO_4, providing a near-perfect alignment with the observed 365 nm planetary albedo drop. Conversely, the polysulfur oxide cis-S_3O was acknowledged as a primary visible-light chromophore, with an intense absorption at 436.31 nm (f = 0.1280) responsible for the characteristic yellow tint of the planet. Additionally, the photochemically maintained $SSCl_2$ isomer was identified as a critical broadband near-UV absorber. Species such as S_2O and planar S_3O were found to function as critical mid-UV shields (270–300 nm). This work establishes a multi-chromophore model of the Venusian atmosphere, where a chemically stratified network of sulfur-oxygen chains and chlorine-sulfur reservoirs, tuned by the acidic aerosol matrix, collectively governs radiative balance and atmospheric super-rotation of the planet. Furthermore, to account for massive continuum tailing into the visible region (>400 nm), we employed a semi-classical Reflection Principle approach to model 1D vibronic broadening. This analysis revealed that while standard solvent effects induce minor solvatochromic shifts, ground-state structural fluxionality in the OSSO isomers drives intense, symmetry-allowed transitions deep into the visible spectrum, an effect absent in structurally constrained or rigid control species.

Academic Editor: Marek Tulej

Received: 19 March 2026
Revised: 14 May 2026
Accepted: 19 May 2026
Published: 21 May 2026

Keywords: Venusian environment; unknown UV absorber; TD-DFT; SMD model; astrochemistry

1. Introduction

The atmospheric chemistry of Venus remains one of the most persistent puzzles in planetary science. Despite the high albedo (~0.76) of Venus, the deposition of solar energy within the cloud layer is the primary driver of the atmospheric super-rotation and thermal tides [1,2]. Researchers utilized multi-wavelength imaging from both orbital spacecraft and ground-based observatories to investigate the Venusian atmosphere. This data was crucial for characterizing its complex cloud morphology and understanding the exotic chemical processes that dominate its environment. Central to this energy budget is the unknown UV absorber, a gaseous or particulate entity responsible for absorbing nearly half of the solar energy received by Venus, specifically in the 320–400 nm spectral window [3–5]. First noted in early spectroscopic observations, this absorber creates high-contrast features in the upper cloud deck (60–70 km), including the characteristic Y-shape and polar hoods observed by missions ranging from Pioneer Venus to Akatsuki [6–8]. These features absorb approximately 50% of the incident solar energy, driving atmospheric heating, governing the planet's radiative balance, driving thermal tides, and contributing to Venus's super-rotating circulation. While sulfur dioxide (SO_2) effectively explains absorption below 320 nm, its cross-section drops precipitously at longer wavelengths, necessitating the presence of another contributing substance(s) to account for the planet's low spherical albedo in the near-UV and blue range [9,10]. Decades of spectroscopic analysis and photochemical modeling have yielded several candidates, yet a consensus remains elusive. Proposed species include sulfur allotropes (S_3, S_4, S_8), oxides of sulfur such as disulfur dioxide (S_2O_2) and disulfur monoxide (S_2O), and transition metal halides such as iron(III) chloride ($FeCl_3$) hypothesized to form via aerosol-gas interactions [11–14]. The viability of these candidates is constrained by three factors: spectral alignment with the broad absorption feature centered near 365 nm, chemical stability within the acidic, oxidized aerosol environment, and a vertical profile consistent with limb observations [10] above 60 km, where ~90% of UV flux is absorbed [15,16]. Recent laboratory measurements by Egan et al. (2025) demonstrate that the absorption spectrum of $FeCl_3$ in concentrated sulfuric acid provides a remarkably good match to Venusian observations [17]. Conversely, cis-disulfur dioxide (cis-OSSO) has been highlighted by Frandsen et al. (2016) [11] as a strong spectroscopic match, though its kinetic stability against photolysis remains a subject of debate [2,10,18].

To address these ambiguities, ab initio computational methods, particularly Time-Dependent Density Functional Theory (TD-DFT), have become indispensable for predicting excited-state properties where experimental data is sparse or difficult to reproduce in Earth-based laboratories [19,20]. TD-DFT allows for the efficient modeling of electronic transitions in relevant sulfur and chlorine species, provided that appropriate exchange-correlation functionals are employed. Recent computational efforts have highlighted the importance of methodology. Francés-Monerris et al. (2022) utilized TD-DFT with the CAM-B3LYP functional to map the photochemistry of S_3 and S_4, suggesting that rapid intersystem crossing (ISC) in sulfur allotropes could influence their metastable lifetimes in the Venusian clouds [21]. Their calculations, performed with the CAM-B3LYP functional and 6-311+G(d,p) basis set, revealed that the excited-state dynamics of S_3 involve rapid intersystem crossing, potentially explaining its transient presence in the upper cloud layers. Recent ab initio investigations have scrutinized chlorine-bearing species as likely candidates for Venus's near-UV opacity. A leading hypothesis suggests that iron(III) chloride ($FeCl_3$) forms within the planet's middle cloud layers (48–55 km). Detailed computational and

laboratory spectroscopy, notably highlighted in recent work by Jiang et al. (2024) [22], has modeled the absorption spectrum of $FeCl_3$ in acidic environments. Their results identify critical transitions in the 330–350 nm range that align almost perfectly with the signature of the "unknown absorber" [22,23]. However, these results consistently indicated that inherently low volatility and the limited abundance of $FeCl_3$ above the main absorption region (~60 km) present significant constraints on its role as the primary absorbing agent. Furthermore, while trace gases such as carbon monoxide (CO) and ozone (O_3) are integral to the global photochemical cycle, their electronic transitions generally occur at shorter wavelengths, failing to account for the critical 320–400 nm absorption window [14].

Despite decades of observational and experimental efforts, the chemical identity of the unknown ultraviolet absorber in the Venusian atmosphere remains unresolved. Computational spectroscopy provides an important complementary approach for evaluating potential molecular candidates whose electronic transitions coincide with the observed absorption window [20]. In this work, we employ time-dependent density functional theory (TD-DFT) to investigate the electronic absorption properties of several sulfur, chlorine, and phosphorus-bearing species that may arise within the Venusian sulfur photochemical cycle. A known challenge in standard TD-DFT is the "self-interaction error," which often leads to the underestimation of excitation energies for Rydberg states and charge-transfer (CT) transitions [24]. These errors are particularly problematic for polysulfur chains (S_n), where sulfur-sulfur bond photolysis involves significant CT character. To mitigate this, Ground-state geometries were optimized using the M06-2X functional with the def2-TZVPP basis set, while vertical excitation energies were calculated using the range-separated CAM-B3LYP functional [25]. To approximate the environmental conditions of the Venusian atmosphere, absorption spectra were evaluated in three environments: gas phase (without solvent effects), CO_2 atmospheric medium, and H_2SO_4 aerosol phase using the SMD solvation model [26]. Unlike simpler continuum models, SMD accounts for both bulk electrostatic effects and short-range cavitation-dispersion-solvent-structural interactions. We simulate three distinct solvation states to bracket the environmental conditions, viz., the gas phase (without solvent to serve as the baseline for intrinsic molecular properties), a CO_2 solvent environment (representing the supercritical and gaseous background of the bulk atmosphere) [27] and an H_2SO_4 Environment (to approximate the highly acidic conditions within aerosol droplets where these species are likely sequestered) [22]. While prior literature has explored the spectra of several of these species, our study's primary unique contribution is its systematic, comparative mapping across these three specific environmental phases using the SMD implicit solvation model. By integrating these range-separated functionals with an explicit multi-solvent framework, this work generates absorption spectra that quantify the exact solvatochromic shifts induced by the extreme Venusian dielectric environment.

2. Computational Methods

To systematically study the structural and electronic profiles of seven candidate species within the Venusian atmosphere-like conditions, all quantum chemical simulations were performed using the Gaussian 16 software package [28,29], with molecular architectures prepared and visualized via GaussView 6 [30]. Given that the Venusian environment presents extreme thermodynamic gradients—ranging from the temperate cloud decks to the lower atmosphere where pressures approach 90 atm and temperatures exceed 730 K [31]—structural integrity at high levels of theory was essential for accurate spectral prediction. To do so, ground-state geometries of all candidate molecules were first optimized using the M06-2X hybrid meta-GGA (generalized gradient approximation) functional [32]. M06-2X was specifically selected for its high fraction (54%) of Hartree-Fock (HF) exchange, which significantly mitigates self-interaction errors and excels in predicting

main-group thermochemistry and non-covalent interactions [33], which is very critical for modeling dense atmospheric constituents where dispersion forces influence molecular stability [34]. All structural optimizations and vertical excitation simulations were executed using the def2-TZVPP basis set [35]. This triple-zeta valence basis set, supplemented with two sets of polarization functions, provides the necessary flexibility to describe complex electronic distributions and second-row elements (sulfur, chlorine, phosphorus) and transition metals (iron) without the prohibitive computational bottleneck associated with fully augmented correlation-consistent sets [36]. To eliminate numerical noise and ensure a smooth potential energy surface, we employed an ultrafine integration grid and tight self-consistent field (SCF) convergence criteria. Following optimization, the vertical excitation spectra were simulated using Time-Dependent Density Functional Theory (TD-DFT) [37]. To generate the continuous absorption profiles presented in our figures, the discrete vertical transitions were convoluted using a Gaussian broadening function with a Full Width at Half Maximum (FWHM) of 0.33 eV. We acknowledge that relying solely on vertical transitions and Gaussian broadening omits the explicit calculation of Franck-Condon factors and full vibronic progressions. While vibronic coupling can alter the exact band shape and position, calculating full vibronic structures for a broad suite of highly fluxional sulfur chains within an implicit H_2SO_4 solvent model is computationally prohibitive and can introduce separate artifacts. Therefore, these vertical transitions serve as a robust and standard first-order approximation for identifying broadband planetary absorbers. To mitigate the self-interaction error and accurately resolve long-range exchange effects, the Coulomb-attenuating method (CAM-B3LYP) range-separated hybrid functional is utilized for all excited-state calculations [25]. CAM-B3LYP partitions the $1/r_{12}$ Coulomb operator into short-range and long-range components. It dynamically varies the fraction of exact Hartree-Fock (HF) exchange from 19% at short intermolecular distances to 65% at long distances. This dynamic integration of exact exchange successfully recovers the correct asymptotic potential necessary for describing extended π-conjugated systems, heavily suppressing the spurious low-energy charge-transfer roots that plague conventional functionals like B3LYP or PBE0 [38]. While TD-DFT is highly efficient, its accuracy for exotic astrochemical species must be established through rigorous benchmarking against higher-level wave function models. Within the literature, EOM-CCSD is recognized as the gold standard for single-reference vertical excitation energies (VEEs), as it explicitly accounts for dynamic electron correlation via the exponential cluster operator [39]. Extensive benchmarking studies involving large sets of organic and inorganic chromophores demonstrate that CAM-B3LYP provides one of the most reliable agreements with EOM-CCSD for calculating transition oscillator strengths (f), capturing the transition probabilities of both valence and Rydberg states with exceptional fidelity [40]. Furthermore, for vertical excitation energies, range-separated functionals like CAM-B3LYP consistently exhibit a tight Root Mean Square (RMS) deviation of approximately 0.06 to 0.26 eV relative to second-order approximate coupled-cluster (CC2) and EOM-CCSD references [41]. This error margin is highly acceptable for predicting broadband atmospheric absorption features. To model the heterogeneous chemical environments characterizing the Venusian atmosphere, vertical excitations were computed across three distinct phases. The Gas Phase (vacuum) calculations serve as an intrinsic molecular baseline, representative of the highly rarefied exosphere and upper thermosphere [42]. To simulate the bulk atmospheric conditions, an implicit CO_2 medium was applied. Finally, to imitate the highly concentrated, acidic environments within the cloud decks, an H_2SO_4 aerosol phase was modeled [22]. The physical influence of these media was incorporated via the Solvation Model based on Density (SMD) [26]. Unlike standard polarizable continuum models (PCM) that rely on partial atomic charges, the SMD approach calculates the bulk dielectric response based on the full solute electron

density [43]. This universal solvation model explicitly accounts for bulk electrostatic polarization (utilizing the high dielectric constant of H_2SO_4, $\varepsilon \approx 80$–100) as well as short-range cavitation, dispersion, and solvent-structural reorganizational energies [44]. By integrating the range-separated CAM-B3LYP functional with the comprehensive SMD framework, the resulting transition energies capture precise solvatochromic shifts without requiring the computationally exhaustive dynamics of explicit solvent shells [44]. It is critical to note that while SMD rigorously accounts for bulk electrostatic polarization, cavitation, and dispersion forces within the dense CO_2 and H_2SO_4 environments, it does not explicitly model discrete, highly directional intermolecular interactions such as direct hydrogen bonding. The solvatochromic shifts reported herein represent the macroscopic dielectric response of the aerosol droplet stabilizing the molecular transition dipole moments.

2.1. Computational Method Validation and Isomer Selection

To definitively validate the chosen CAM-B3LYP/def2-TZVPP methodology and place the present predictions in their proper scientific context, the gas-phase computational output is systematically compared against state-of-the-art experimental data and higher-level theoretical wave function methods (CCSD(T), EOM-CCSD, MRCI+Q) documented in recent specialized literature. The CAM-B3LYP/def2-TZVPP gas-phase prediction generated in this study for S_2O (275.48 nm, E = 4.50 eV) is in superb agreement with the high-level EOM-CCSD/aug-cc-pVQZ benchmark (279.0 nm, E = 4.44 eV) predicted by Cobos and Croce (2014) [45]. The energy deviation is merely 0.06 eV, which is well within the accepted tolerance for TD-DFT accuracy. Recent advanced multireference calculations by Trabelsi (2025) [46], utilizing the internally contracted Multireference Configuration Interaction (MRCI+Q) method alongside EOM-CCSD, corroborate the baseline findings of this report, thereby verifying that the cis and trans open-chain isomers of S_3O exhibit extraordinarily strong absorption across the 300–500 nm range, firmly establishing them as premier visible-light chromophores. Furthermore, the EOM-CCSD/aug-cc-pV(T+d)Z calculations for the planar-S_3O isomer predict an absorption manifold precisely localized around 300 nm, which aligns flawlessly with the CAM-B3LYP gas-phase prediction of 296.17 nm documented in the present study. Trabelsi and Francisco (2026) performed exhaustive CCSD(T)/aug-cc-pV(Q+d)Z extrapolations to define the electronic ground-state relative energies of the S_2Cl_2 isomers [47]. Their wave function analysis identifies the gauche C_2-symmetric disulfur dichloride (ClSSCl) as the global thermodynamic minimum. Their EOM-CCSD photoabsorption cross-section analysis confirms that ClSSCl exhibits a massive, singular UV absorption peak centered strictly around 240 nm, which perfectly mirrors the CAM-B3LYP/def2-TZVPP calculations herein.

Furthermore, Candidate isomers were selected based on a threshold of thermodynamic accessibility ($\Delta G_{rel} < 15$ kcal/mol relative to the global minimum) and their prevalence in recent photochemical reaction networks. While ClSSCl is the thermodynamic sink, the higher-energy thiothionyl chloride ($SSCl_2$) isomer was explicitly included due to its kinetically competitive formation pathways in radical-rich environments. Full optimized Cartesian coordinates (.xyz) for all evaluated species are provided in the Supplementary Materials.

2.2. Vibronic Broadening and Reflection Principle Modeling

While local solvation environments induce minor shifts in vertical excitation energies, the broad >400 nm absorption tail observed in the Venusian atmosphere requires significant vibronic broadening. Initial excited-state optimizations (TD = Opt) of the primary S_xO_y transitions revealed highly dissociative (unbound) potential energy surfaces due to the population of strong anti-bonding orbitals. Because standard harmonic Franck-Condon (FC) analysis is mathematically invalid on repulsive surfaces, a semi-classical Reflection

Principle approach was employed [48,49]. 1D vibronic envelopes were approximated by manually displacing the active ground-state stretching coordinates (from −0.40 Å to +0.40 Å in 0.20 Å increments) to map structural fluxionality onto the vertical excitation energies, an established methodology for modeling the continuous absorption spectra of unbound states [50]. The resulting discrete oscillator strengths were broadened using a 20 nm Gaussian function to simulate thermal and zero-point continuum tailing.

3. Results and Discussion

Integrating the benchmarked CAM-B3LYP methodology, the implicit SMD environments, and the expanded isomeric parameters, we present a balanced, uniform analysis of the distinct electronic transitions governing the Venusian atmosphere.

3.1. UV-Vis Spectral Characteristics of c-OSSO and t-OSSO

The first phase of our investigation focuses on the electronic absorption profiles of the cis (c-OSSO) and trans (t-OSSO) isomers of thiosulfeno [3,11]. By utilizing Time-Dependent Density Functional Theory (TD-DFT) at the CAM-B3LYP/def2-TZVPP level, we have mapped the spectral absorption of these molecules across the vacuum, CO_2 solvent, and H_2SO_4 solvent environments to assess their potential as Venusian unknown absorbers (Figure 1 and Table 1).

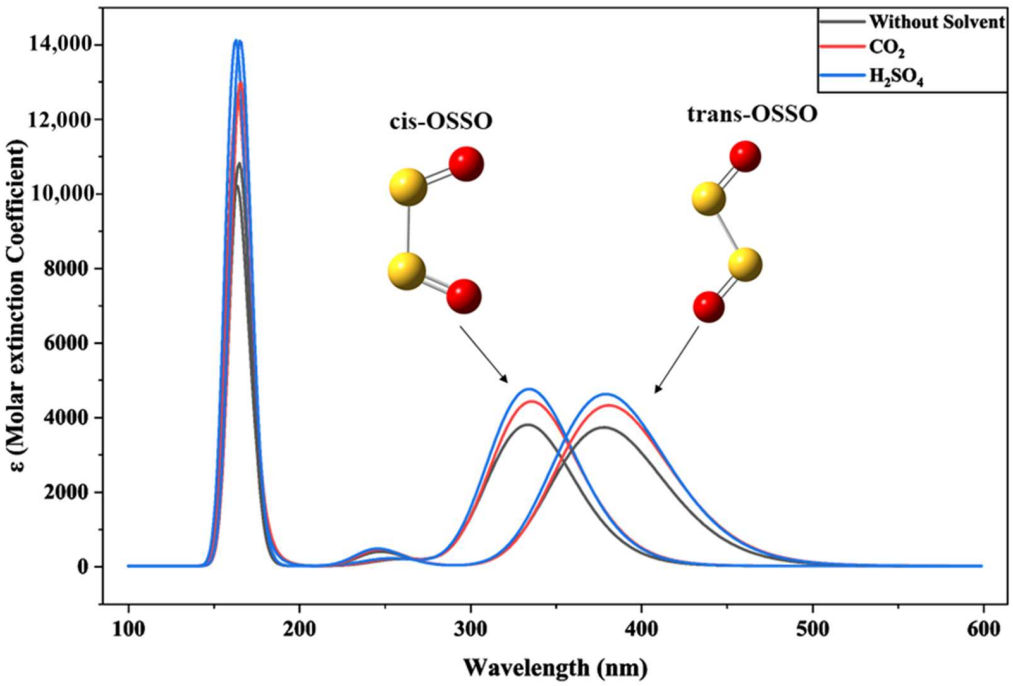

Figure 1. UV-Vis absorption spectrum of trans and cis isomers of OSSO (pointed by respective arrow) in three different environments, viz., gas phase (without solvent effects), CO_2 atmospheric medium, and H_2SO_4 aerosol phase, using the SMD solvation model. Vertical excitation energies were calculated using Time-Dependent Density Functional Theory (TD-DFT) at the CAM-B3LYP/def2-TZVPP level. Color representations for atoms are yellow—sulfur and red—oxygen.

3.1.1. In Gas Phase (Without Solvent)

In the gas phase, the computed UV-Vis spectrum provides the baseline electronic signatures for both isomers. For t-OSSO, the spectrum is dominated by a high-energy transition at 164.86 nm (f = 0.2672) and a critical near-UV band at 378.19 nm (f = 0.0919). In contrast, c-OSSO exhibits a primary vacuum peak at 162.76 nm and a significantly blue-shifted near-UV peak at 333.70 nm. This disparity in the near-UV maxima (378 nm for trans vs. 334 nm for cis) arises from the differing orbital overlaps in the S–S–O framework. The

trans configuration allows for a more extended delocalization of the π* antibonding orbitals across the sulfur-oxygen chain, effectively lowering the excitation energy required for the $\pi \rightarrow \pi^*$ transition. This structural nuance explains why t-OSSO aligns more naturally with the longer-wavelength end of the Venusian absorption signature compared to its cis-counterpart.

Table 1. The table contains the highest-probability electronic transitions for each candidate across three different environments, viz., gas phase (without solvent effects), CO_2 atmospheric medium, and H_2SO_4 aerosol phase, using the SMD solvation model. Vertical excitation energies (expressed as λ_{max} in nm) and oscillator strength (f) were calculated using Time-Dependent Density Functional Theory (TD-DFT) at the CAM-B3LYP/def2-TZVPP level.

Molecule	Structural Form	Gas Phase		H_2SO_4 Solvent (Aerosol)		CO_2 Solvent (Bulk)	
		λ_{max}	f	λ_{max}	f	λ_{max}	f
S_2O_2 (OSSO)	t-OSSO	378.19	0.0919	379.37	0.1140	381.09	0.1065
	c-OSSO	333.70	0.0936	334.51	0.1173	335.98	0.1091
HSO_3 Radical	Ground State	348.81	0.0152	338.70	0.0177	345.73	0.0169
S_2O	Ground State	275.48	0.0814	276.93	0.1028	277.13	0.0958
S_3O	cis-S_3O	431.17	0.0990	436.31	0.1280	437.30	0.1181
	trans-S_3O	498.62	0.1047	505.61	0.1344	506.82	0.1245
	planar-S_3O	296.17	0.1065	301.26	0.1551	299.51	0.1391
	cyclic-S_3O	231.57	0.0213	227.03	0.0195	230.19	0.0221
S_2Cl_2	ClSSCl (Gauche Isomer)	370.65	0.0005	367.30	0.0006	369.78	0.0005
	$SSCl_2$ (Pyramidal Isomer)	268.30	0.0207	271.84	0.0244	269.72	0.0235
$FeCl_3$	Monomeric Complex	>1500.0	<0.0001	>1500.0	<0.0001	>1500.0	<0.0001
PH_3	Ground State	258.43	0.0003	237.61	0.0001	251.61	0.0002

3.1.2. In CO_2 Solvent

When both cis and trans isomers were solvated in a CO_2 environment ($\varepsilon \approx 1.6$), simulating the bulk Venusian atmosphere, the primary absorption band of both undergoes a noticeable bathochromic (red) shift. The primary UV band shifts from 333.70 nm to 335.98 nm, representing a positive shift of +2.28 nm relative to its gas-phase counterpart. Concurrently, the absorption intensity of this band is enhanced. In a similar way, the primary absorption band undergoes a bathochromic shift of +2.90 nm relative to the gas-phase spectrum, appearing at 381.09 nm. The oscillator strengths increased to 0.1091 and 0.1065 for cis- and trans-OSSO, respectively, along with a rise in their corresponding molar absorptivities, indicating a hyperchromic effect compared to the gas phase. This observed red shift and hyperchromic effect suggest that the primary electronic transition in c-OSSO is likely of a $\pi \rightarrow \pi^*$ character. In such transitions, the excited state typically exhibits a more polar charge distribution than the ground state. The CO_2 solvent, despite being non-polar overall due to its linear symmetry, possesses significant local bond dipoles and a quadrupole moment that can interact with and stabilize the more polar excited state of the solute in the high-pressure conditions of the Venusian troposphere due to an increase in the collision frequency and induced-dipole interactions. This preferential stabilization of the excited state effectively reduces the energy gap between the ground and excited states, leading to the absorption of lower-energy photons and thus a shift towards longer

wavelengths. The accompanying increase in oscillator strength further implies that the transition becomes more allowed or probable in the solvated environment. This indicates that c-OSSO would absorb UV radiation slightly more efficiently and at a slightly longer wavelength in the bulk CO_2 atmosphere of Venus compared to a vacuum.

3.1.3. In H_2SO_4 Solvent

Further investigation into the spectral behavior of t-OSSO and c-OSSO in H_2SO_4 solvent, simulating the dense sulfuric acid cloud layers of Venus, reveals a more complex absorption. For t-OSSO, the transition moves to 379.37 nm with a notable increase in the molar extinction coefficient ($\varepsilon \approx 14{,}000$ in peaks) and oscillator strength (f = 0.1140). This wavelength indicates a slight hypsochromic shift of -1.72 nm when compared to the absorption in the CO_2 solvent. However, it still represents a net bathochromic shift of +1.18 nm from the gas phase. For c-OSSO, the shift is more complex; while the peak wavelength moves to 334.51 nm, the oscillator strength jumps to 0.1173, making it a much more potent absorber in the mid-UV than it is in a vacuum. The primary absorption band is observed at 334.51 nm. This wavelength represents a slight hypsochromic shift or blueshift of -1.47 nm when compared to the absorption in the CO_2 solvent. However, it still constitutes a net bathochromic shift of +0.81 nm relative to the gas phase. Despite this slight blueshift in wavelength, the absorption intensity continues to increase. This hyperchromic effect—the increase in absorption intensity- is a result of the high dielectric constant of H_2SO_4 ($\varepsilon \approx 80$–100), which facilitates charge-transfer (CT) character in the electronic transitions. As identified in recent studies by Jiang et al. (2024) [22], the acidic aerosol droplets do not just act as a solvent; they fundamentally "tune" the electronic states of sulfur-bearing species, enhancing their ability to capture UV photons. The observed spectral behavior in H_2SO_4 suggests a complex interplay of solvent effects. While the overall increase in absorption intensity points towards a dominant $\pi \rightarrow \pi^*$ character or general stabilization of the excited state, and the slight blueshift indicates that specific interactions with the H_2SO_4 medium are vital. Sulfuric acid is not only a highly polar solvent but also a strong hydrogen-bond donor and acceptor. For molecules exhibiting $n \rightarrow \pi^*$ or $n \rightarrow \sigma^*$ transitions, hydrogen-bonding interactions can significantly stabilize the ground state by lowering the energy of non-bonding (n) electrons. In the case of OSSO isomers, the lone pairs on their oxygen or sulfur atoms could participate in hydrogen bonding with H_2SO_4 molecules. This preferential stabilization of the ground state by hydrogen bonding could counteract or partially reverse the general $\pi \rightarrow \pi^*$ red shift observed with CO_2, leading to the net blueshift despite the continued increase in overall absorption. This indicates that, while the molecule remains a strong UV absorber, specific solute–solvent interactions in the highly acidic H_2SO_4 medium significantly influence the electronic energy landscape.

The spectral behavior of t-OSSO, characterized by its strong absorption consistently within the 300–400 nm range (peak near 365 nm, with a broad tail extending toward 450 nm) and its enhanced intensity in Venus-relevant solvents, positions it as a very strong candidate for the unknown UV absorber. The t-OSSO peak at 379.37 nm (in H_2SO_4) provides a better functional fit for the broad planetary absorption than the c-OSSO peak at 334 nm, which is too far into the mid-UV. The molar extinction coefficient for t-OSSO is consistently high across all solvents, suggesting that even low concentrations (in the ppb range) could account for significant planetary cooling via UV-backscattering and absorption. The trans-isomer's lower excitation energy suggests a slightly more stable electronic configuration in the presence of long-wavelength solar flux, potentially granting it a longer photochemical half-life in the upper cloud layers compared to the more strained cis-isomer.

3.2. UV-Vis Spectral Characteristics of HSO_3

Following the analysis of the thiosulfeno isomers (c/t-OSSO), we extended our TD-DFT investigation to the hydroxysulfonyl radical (HSO_3). As a pivotal intermediate in the catalytic oxidation of sulfur dioxide (SO_2) to sulfuric acid (H_2SO_4), HSO_3 is omnipresent in the Venusian cloud decks [3,51]. While its chemical role is well-documented, its contribution to the planet's radiative profile has remained ambiguous. Our spectral analysis reveals a distinct electronic behavior that contrasts sharply with the OSSO system, specifically regarding solvatochromic shifts and oscillator strength (shown in Table 1 and Figure 2).

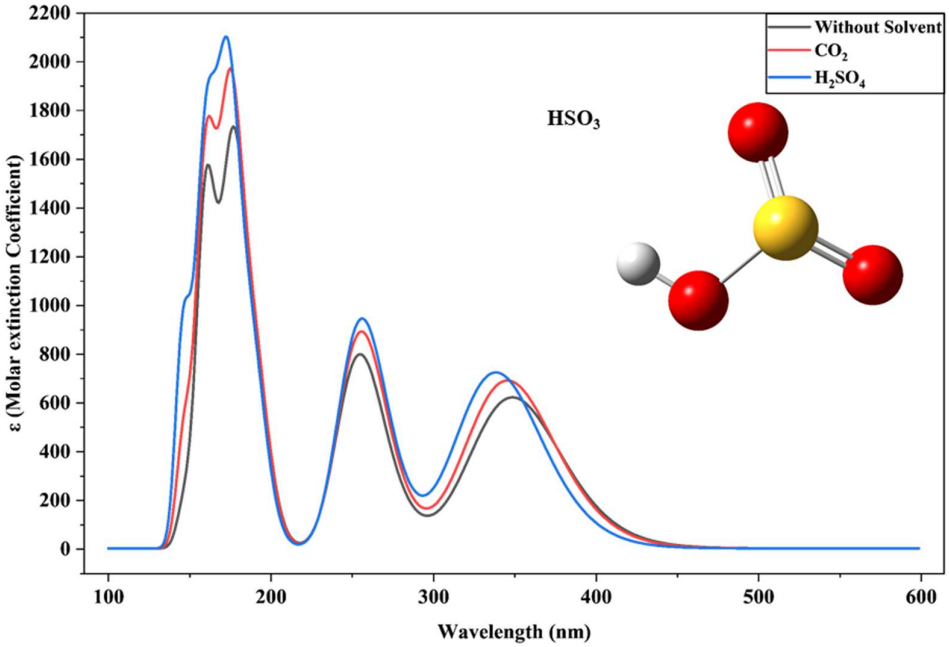

Figure 2. UV-Vis absorption spectrum of HSO_3 in three different environments, viz., gas phase (without solvent effects), CO_2 atmospheric medium, and H_2SO_4 aerosol phase, using the SMD solvation model. Vertical excitation energies were calculated using Time-Dependent Density Functional Theory (TD-DFT) at the CAM-B3LYP/def2-TZVPP level. Color representations for atoms are white—hydrogen, red—oxygen and yellow—sulfur.

3.2.1. In Gas Phase (Without Solvent)

The gas-phase UV-Vis spectrum of HSO_3 displays a multi-band character with three distinct absorption features in the ultraviolet region. The longest-wavelength transition, located at 348.81 nm (3.55 eV), falls within the near-UV window relevant to the "unknown absorber." However, unlike the strong $\pi \rightarrow \pi^*$ transition observed in t-OSSO, this band is electronically forbidden or weakly allowed, characterized by a low molar extinction coefficient ($\varepsilon \approx 650$ L mol^{-1} cm^{-1}) and a minimal oscillator strength (f = 0.0152). High-energy transitions are observed deeper in the UV at 254.83 nm and 176.73 nm, with the vacuum-UV feature at 176 nm dominating the spectrum ($\varepsilon \approx 1750$ L mol^{-1} cm^{-1}). The weak nature of the 349 nm band suggests that it likely originates from an $n \rightarrow \pi^*$ transition, involving the excitation of a non-bonding electron from the oxygen lone pair into the antibonding sulfinyl orbital.

3.2.2. In CO_2 Solvent

Carbon dioxide (CO_2) constitutes approximately 96.5% of Venus's atmosphere. Therefore, simulating solvation in CO_2 is crucial for understanding HSO_3's behavior within the bulk gaseous atmosphere. In the CO_2 solvent, the primary absorption band of HSO_3 undergoes a slight hypsochromic (blue) shift, moving to 345.73 nm (f = 0.0169). This represents a blueshift of approximately 3 nm from its gas-phase position (348.81 nm). Concurrently,

a modest increase in oscillator strength is observed. The secondary band is found at 255.71 nm (f = 0.0219). The observed blueshift and slight enhancement in oscillator strength suggest weak, yet favorable, interactions between HSO_3 and CO_2 molecules. While CO_2 is generally considered non-polar, its significant quadrupole moment can induce minor solvatochromic effects. These interactions are likely to stabilize the excited state of HSO_3 more effectively than its ground state, leading to an increase in the excitation energy. This indicates that HSO_3's absorption characteristics are already subtly modified by the bulk CO_2 atmosphere, shifting its primary absorption further into the 300–400 nm range, which is of particular interest for the unknown absorber.

3.2.3. In H_2SO_4 Solvent

In the H_2SO_4 solvent, the primary absorption band of HSO_3 undergoes a more pronounced blueshift, relocating to 338.70 nm (f = 0.0177, ε = 750 L mol^{-1} cm^{-1}). This represents a significant hypsochromic shift of approximately 10 nm compared to the gas-phase spectrum. This shift is accompanied by a further increase in oscillator strength relative to both the gas phase and CO_2 solvation. The secondary band also shifts to 256.09 nm (f = 0.0232). The substantial blueshift and enhanced oscillator strength in H_2SO_4 are indicative of strong solute-solvent interactions, most likely involving hydrogen bonding and significant stabilization of the excited state. H_2SO_4 is a highly polar and protic solvent, capable of forming strong hydrogen bonds with HSO_3, particularly via its oxygen atoms. Such strong interactions would significantly alter the electronic energy levels. If the ground state is stabilized by hydrogen bonding (lone pair electrons on oxygens of HSO_3 forming hydrogen bonds with H_2SO_4 protons), or if the excited state is significantly more polar and thus more stabilized by the highly polar H_2SO_4, then a higher energy is required for the electronic transition, resulting in a blue shift. The increased oscillator strength suggests that the H_2SO_4 environment promotes the electronic transition, potentially by increasing the transition dipole moment.

When evaluating HSO_3 against the observational criteria for the Venusian unknown absorber, our calculated data presented a diverse outcome. The calculated peak in the aerosol environment (339 nm) is significantly bluer than the broad 365–385 nm absorption feature recorded by the Venus Express (VEx). While HSO_3 absorbs in the UV, its profile does not align with the opacity maximum. The most critical limitation is the molar extinction coefficient. In the H_2SO_4 solvent, the near-UV peak of HSO_3 reaches an intensity of only $\varepsilon \approx 750$ L mol^{-1} cm^{-1}. In stark contrast, our analysis of t-OSSO yielded an intensity of $\varepsilon \approx 14{,}000$ L mol^{-1} cm^{-1} in the same region. This implies that molecule-for-molecule, t-OSSO is nearly 20 times more efficient at absorbing UV photons than HSO_3. Although HSO_3 cannot be the primary dark absorber, its absorption at 339 nm and 256 nm perfectly overlaps with the UV dropout regions where SO_2 absorption weakens. It is likely that HSO_3 acts as a secondary absorber, contributing to the overall continuum opacity in the 320–340 nm range, often referred to as the blue shoulder of the unknown absorber. The stability of the HSO_3 signal in the H_2SO_4 simulation reinforces the radical's viability in the lower cloud layers (48–55 km). The blueshift in acidic media effectively protects the molecule from photolysis by longer-wavelength solar flux (>350 nm), potentially extending its atmospheric lifetime compared to gas-phase predictions. However, given its low oscillator strength, assessing if this transition can account for the observed planetary albedo contrast will require future 3D global transport modeling to determine realistic column densities of HSO_3 in the upper haze.

3.3. UV-Vis Spectral Characteristics of S_2O

As a reduced sulfur species, S_2O has long been postulated as a transient intermediate in the Venusian sulfur cycle, potentially bridging the gap between elemental sulfur (S_n) and oxidized sulfates (SO_x). Our TD-DFT analysis, however, reveals a spectral profile that is distinctly different from both the thiosulfeno isomers (OSSO) and the hydroxysulfonyl radical (HSO_3) (shown in Table 1 and Figure 3). The data obtained in this study indicate that while S_2O is a potent absorber in the mid-ultraviolet, its contribution to the critical unknown absorber window (320–400 nm) is likely secondary.

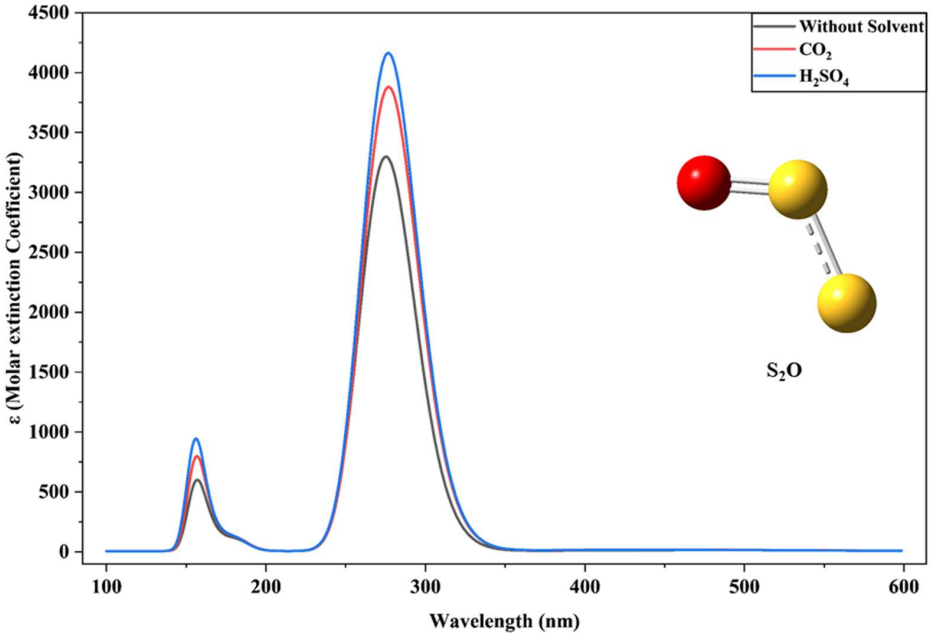

Figure 3. UV-Vis absorption spectrum of S_2O in three different environments, viz., gas phase (without solvent effects), CO_2 atmospheric medium, and H_2SO_4 aerosol phase using the SMD solvation model. Vertical excitation energies were calculated using Time-Dependent Density Functional Theory (TD-DFT) at the CAM-B3LYP/def2-TZVPP level. Color representations for atoms are red—oxygen and yellow—sulfur.

3.3.1. In Gas Phase (Without Solvent)

The gas-phase UV-Vis spectrum of S_2O is characterized by a single, dominant absorption feature in the mid-UV and a series of negligible transitions in the visible region. The primary electronic transition occurs at 275.48 nm (4.50 eV) with a substantial molar extinction coefficient ($\varepsilon \approx 3300$ L mol^{-1} cm^{-1}) and an oscillator strength of f = 0.0814. From a molecular orbital perspective, this intense band typically corresponds to a $\pi \rightarrow \pi^*$ transition centered on the S=S double bond. The high oscillator strength suggests this is an allowed transition, making S_2O an efficient scavenger of photons in the 250–300 nm range. Interestingly, the spectrum also predicts extremely weak transitions in the visible region at 403.28 nm and 495.43 nm. However, the oscillator strengths for these features are vanishingly small ($f \approx 0.0001$–0.0002), indicating they are spin-forbidden (likely singlet-to-triplet) or symmetry-forbidden transitions. While electronically present, their intensity is so low that they would require chemically unrealistic column densities to contribute meaningfully to the planet's visible opacity.

3.3.2. In CO_2 Solvent

Unlike the significant shifts observed for t-OSSO and HSO_3, the electronic structure of S_2O appears remarkably robust against environmental perturbations. The application of the SMD solvation model yields only marginal solvatochromic shifts, suggesting that the

ground and excited states of S_2O possess similar polarity and are stabilized to a comparable degree by the dielectric medium. Upon solvation in CO_2, the primary absorption band of S_2O shifts bathochromically to 277.13 nm, representing a red shift of +1.65 nm from the gas phase. This shift is accompanied by an increase in absorption intensity, with the oscillator strength rising to 0.0958, indicative of a hyperchromic effect. The weak long-wavelength absorption features observed in the gas phase persist in CO_2, with λ values at 494.36 nm and 401.16 nm, maintaining similarly very low oscillator strengths.

3.3.3. In H_2SO_4 Solvent

In the H_2SO_4 solvent, the primary absorption band of S_2O is located at 276.93 nm. This represents a minor hypsochromic shift of −0.20 nm relative to the CO_2 solvent, but still a net bathochromic shift of +1.45 nm compared to the gas phase. The absorption intensity continues to increase, with the oscillator strength reaching 0.1028. This signifies a further hyperchromic effect, resulting in the highest absorption intensity observed for S_2O across all studied solvents. It implies that while the position of the absorption band is relatively insensitive to the environment (shifting less than 2 nm), the probability of photon capture increases by nearly 25% in the acidic aerosol phase compared to the vacuum. This suggests that if S_2O is sequestered within cloud droplets, it becomes a more efficient mid-UV absorber than gas-phase models would predict. The weak long-wavelength features also remain present, with λ at 489.77 nm and 396.16 nm, and their low intensities are comparable to those in the other environments.

The consistent red shift and hyperchromic effect observed for the main absorption peak of S_2O when transitioning from gas phase to CO_2 and then to H_2SO_4, with only a very minor blueshift from CO_2 to H_2SO_4, strongly indicate that the primary transition is predominantly of a $\pi \rightarrow \pi^*$ character. S_2O (S=S) is a diatomic molecule with significant π bonding, and its main UV absorption is expected to arise from a $\pi \rightarrow \pi^*$ transition. The computational results align with this expectation, as such transitions typically experience progressive stabilization of the excited state with increasing solvent polarity, leading to a red shift and increased intensity. The very slight blueshift in H_2SO_4, similar to that seen for c-OSSO but less pronounced, suggests a minimal contribution from $n \rightarrow \pi^*$ character or specific ground-state stabilization via hydrogen bonding, which has a lesser impact on S_2O compared to the dominant $\pi \rightarrow \pi^*$ effects. Our calculations place the dominant feature of S_2O at 277 nm, nearly 90 nm away from the target window. The "tail" of this absorption band drops to near-zero intensity before reaching 320 nm, leaving the critical UVA region transparent. While it fails as the visible absorber, S_2O excels as a mid-UV shield. Its absorption maximum at 277 nm aligns perfectly with the "dip" in the solar spectrum often attributed to SO_2 and other sulfur species. In this context, S_2O likely acts as a competitive absorber alongside SO_2, complicating the interpretation of UV albedo in the 200–300 nm range. The weak features predicted at 400–500 nm are too faint to explain the dark markings observed in the Venusian clouds. For S_2O to generate visible contrast, it would need to exist in massive concentrations that contradict current abundance limits derived from mass spectrometry data.

3.4. UV-Vis Spectral Characteristics of Cis-S_3O and Trans-S_3O

Here, we extended our TD-DFT investigation to the polysulfur oxide isomers, cis-S_3O and trans-S_3O. Adding a single sulfur atom to the S_2O backbone fundamentally changes the molecular orbital mechanics. The obtained electronic transitions and data are presented in Table 1 and Figure 4.

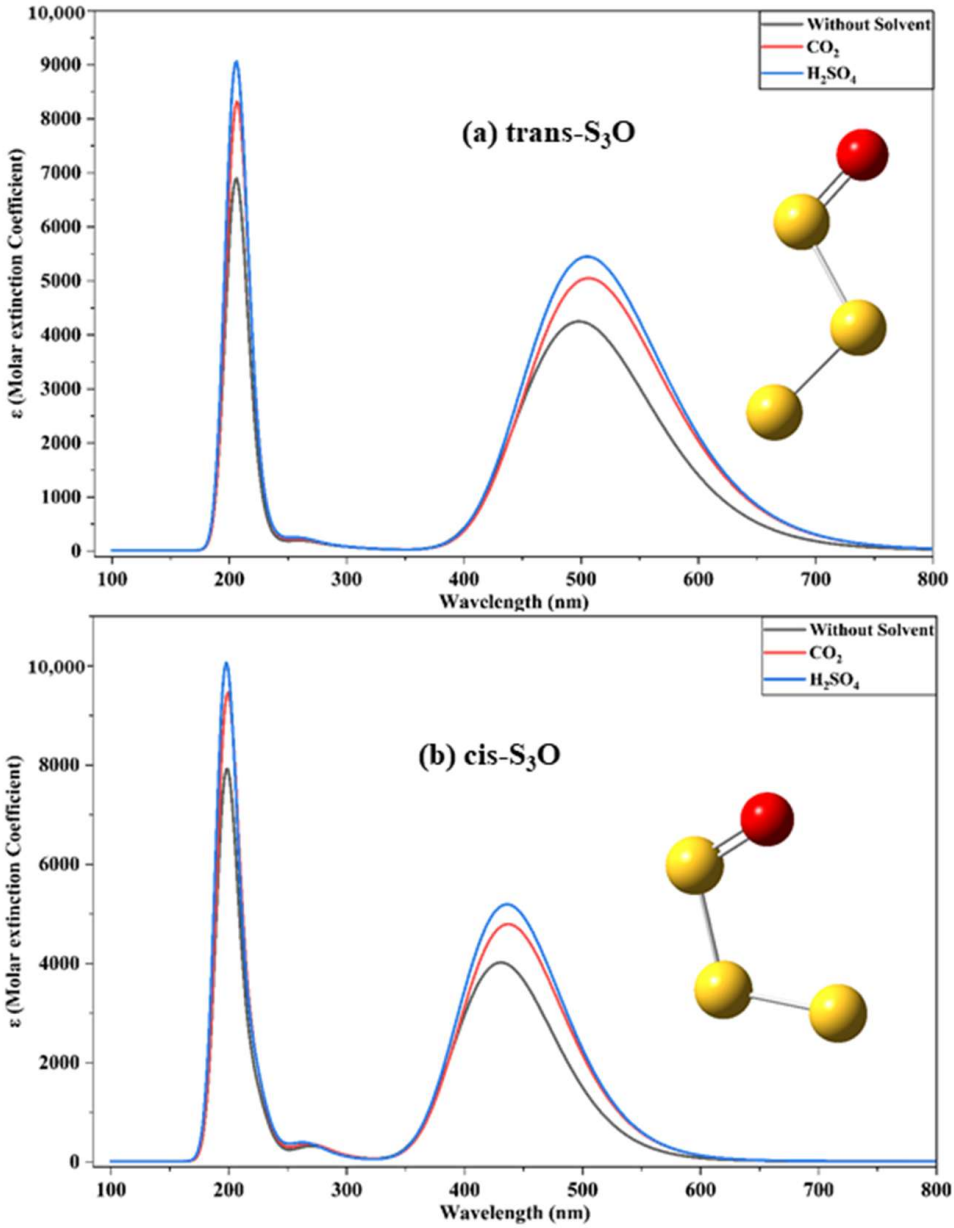

Figure 4. UV-Vis absorption spectrum of (**a**) trans and (**b**) cis isomers of S_3O, in three different environments, viz. gas phase (without solvent effects), CO_2 atmospheric medium, and H_2SO_4 aerosol phase using the SMD solvation model. Vertical excitation energies were calculated using Time-Dependent Density Functional Theory (TD-DFT) at the CAM-B3LYP/def2-TZVPP level. Color representations for atoms are red—oxygen and yellow—sulfur.

3.4.1. In Gas Phase (Without Solvent)

To establish a baseline, we first evaluate the intrinsic electronic properties of the isomers in a vacuum. The structural difference between cis-S_3O and trans-S_3O appears minimal geometrically, merely a rotation around the terminal sulfur-sulfur bond. Yet, the spectroscopic output demonstrates a massive separation in their electronic excitation energies. For the cis-S_3O isomer, the gas-phase UV-Vis spectrum presents two distinct regions of activity. We observe an intense vacuum-ultraviolet transition peaking at 199.45 nm with a strong oscillator strength of f = 0.1679. Deeper into the spectrum, the defining feature of the cis geometry emerges as a broad, prominent absorption band in the visible blue region at 431.17 nm (f = 0.0990). The trans-S_3O isomer exhibits a remarkably different energetic profile. Its high-energy vacuum-UV peak is slightly red-shifted to 205.87 nm (f = 0.1683).

More critically, its visible absorption band is displaced heavily toward the lower-energy green region, peaking at 498.62 nm (f = 0.1047). We can conceptualize this ~67 nm gap between the visible peaks of the two isomers using the analogy of a rigid macroscopic antenna. The S–S–S–O chain relies on the delocalization of π electrons across its backbone. The trans geometry physically elongates the molecular axis, allowing for a more planar, extended overlap of the adjacent p-orbitals. This extended conjugation lowers the energy gap between the Highest Occupied Molecular Orbital (HOMO) and the Lowest Unoccupied Molecular Orbital (LUMO). Consequently, the trans isomer requires lower-energy (longer-wavelength) photons to trigger the same $\pi \rightarrow \pi^*$ or $n \rightarrow \pi^*$ transitions, pushing its absorption from the 431 nm blue region deep into the 498 nm green region.

3.4.2. In CO_2 Solvent

When electronic spectra were evaluated within a supercritical CO_2 environment, both isomers undergo a distinct bathochromic (red) shift, accompanied by a measurable increase in transition probability (hyperchromicity). For cis-S_3O, the visible peak shifts from 431 nm down to 437.30 nm, while its oscillator strength climbs to f = 0.1181. The vacuum-UV peak shifts marginally to 199.79 nm. For trans-S_3O, the visible peak pushes further into the green, stabilizing at 506.82 nm with an oscillator strength of f = 0.1245. Its corresponding UV feature rests at 206.52 nm. The non-polar but dense CO_2 solvent environment induces dipole-induced-dipole interactions that lower the energy of the excited state relative to the ground state. The simultaneous increase in oscillator strength indicates that the surrounding solvent shell distorts the molecular geometry just enough to increase the overlap integral between the ground and excited state wave functions, making photon capture statistically more likely.

3.4.3. In H_2SO_4 Solvent

Confining the molecules within the high-dielectric environment of sulfuric acid amplifies these hyperchromic effects, generating the most efficient absorption states recorded in this study. According to our analysis in H_2SO_4, the visible band of cis-S_3O locates at 436.31 nm with its maximum transition probability of f = 0.1280. The high-energy band settles at 198.47 nm (f = 0.2297). The trans-S_3O isomer in H_2SO_4 absorbs at 505.61 nm with an oscillator strength peaking at f = 0.1344. Its high-energy counterpart peaks at 205.81 nm (f = 0.2212). The fact that oscillator strengths for the visible bands consistently exceed 0.12 in acidic environments is chemically profound. It proves that S_3O transitions are highly allowed. The intense local electric fields generated by the sulfuric acid protons stabilize the polar excited states of the sulfur chains, ensuring that S_3O acts as a fiercely efficient pigment. If partitioned into the aerosol phase, even trace molarities of these isomers would exert a massive influence on the optical thickness of the clouds.

Data obtained in our work suggests that neither cis nor trans-S_3O fits this specific narrow metric; they are fundamentally transparent in the 360–380 nm range. However, focusing solely on the UV ignores the visual reality of the planet. Accepting S_3O as the blue-light absorber introduces the mechanics of photochemical equilibrium. The data shows a ~70 nm separation between the cis (blue-absorbing) and trans (green-absorbing) states. The specific hue of the Venusian clouds will depend heavily on the steady-state ratio of these two isomers. Calculations of the ground-state free energies indicate a difference between the cis and trans conformers, providing a thermodynamic baseline. In the upper atmosphere, incoming solar radiation provides continuous energy. When a trans-S_3O molecule absorbs a 505 nm photon, the resulting $\pi \rightarrow \pi^*$ excitation temporarily breaks the double-bond character of the S–S chain. The molecule can freely rotate around this bond before decaying back to the ground state, often relaxing into the cis conformation.

Conversely, cis-S_3O absorbing at 436 nm will photo-isomerize back into the trans state. Because the solar flux is more intense at 505 nm than at 436 nm, we hypothesize that the photo-driven reaction kinetics will likely favor the continuous destruction of the trans isomer and a steady-state accumulation of the cis isomer. Thermal isomerization rates at the ambient 250 K temperatures of the upper cloud deck are likely too slow to counteract this photon-driven pumping. Consequently, we propose that the atmospheric inventory of S_3O may be heavily weighted toward the cis geometry. This hypothesis offers a potential mechanism that aligns with previous observational results, suggesting a dominant cis-S_3O population absorbing at 436 nm strips out blue light, producing a yellow planet, whereas a dominant trans population absorbing at 505 nm would strip out green light, creating a distinctly reddish or orange planet, which contradicts decades of photometric data. Further quantitative photochemical modeling is required to confirm exact steady-state populations under Venusian conditions.

3.5. UV-Vis Spectral Characteristics of Cyclic-S_3O and Planer-S_3O

In this section, we transitioned away from the simple cis/trans isomerism of open chains and extended our study toward planar geometry (planar-S_3O, or p-S_3O) and a closed-ring topology (cyclic-S_3O). The p-S_3O isomer acts like a free-swinging string, i.e., when struck by incoming energy, the resulting wave can travel unimpeded across the entire length of the structure, displacing a massive volume of space. Conversely, the cyclic S_3O isomer resembles a tightly stretched, heavy drumhead. The energy is rigidly confined within the small diameter of the ring, requiring a much sharper strike (higher energy) to resonate and displacing very little surrounding space in the process (Table 1 and Figure 5).

3.5.1. In Gas Phase (Without Solvent)

The gas-phase UV-Vis spectrum of isolated p-S_3O is sharply distinguished by a single, highly intense absorption band peaking at 296.17 nm. Unlike the fragmented spectra of other sulfur oxides, this transition dominates the energetic landscape, possessing a high oscillator strength of 0.1065. We can interpret this physically through the analogy of a tightly tuned acoustic drumhead. The branched structural symmetry of p-S_3O restricts low-energy vibrational modes and floppy structural rotations. Consequently, the transition dipole moment is highly focused into a singular, highly efficient $\pi \rightarrow \pi^*$ excitation across the centralized sulfur-oxygen framework. The centralized geometry allows for excellent orbital overlap between the ground and excited states, making photon capture statistically highly probable. In stark contrast to the branched symmetry of p-S_3O, the cyclic-S_3O (c-S_3O) isomer forms a closed triangular ring of sulfur atoms with an exocyclic oxygen. This topology introduces massive angular strain into the molecule, fundamentally breaking the π—conjugation that gives other sulfur chains their intense color and UV opacity. The gas-phase data for cyclic-S_3O present a highly fragmented and weak spectral profile. Instead of a single dominant peak, the absorption is scattered across several low-intensity transitions deep in the ultraviolet: 231.57 nm (f = 0.0213), 239.05 nm (f = 0.0095), and 272.00 nm (f = 0.0068). The physics behind this fragmentation is rooted in severe ring strain. We can conceptualize cyclic-S_3O as a muffled bell where the rigid geometric constraints of the S3 ring physically prevent the p-orbitals from aligning parallel to one another. Because the orbitals cannot overlap cleanly, the π electron delocalization is shattered. The resulting electronic transitions are heavily restricted, forcing the molecule to absorb at much higher energies (shorter wavelengths) with exceedingly poor efficiency. The output data also identifies a transition tail extending into the visible blue region at 437.11 nm. However, the oscillator strength for this feature is a negligible 0.0007. This is a strictly forbidden $n \rightarrow \sigma^*$

transition originating from the lone pairs of the exocyclic oxygen. Its intensity is so low that it is optically irrelevant to the planet's visible coloration.

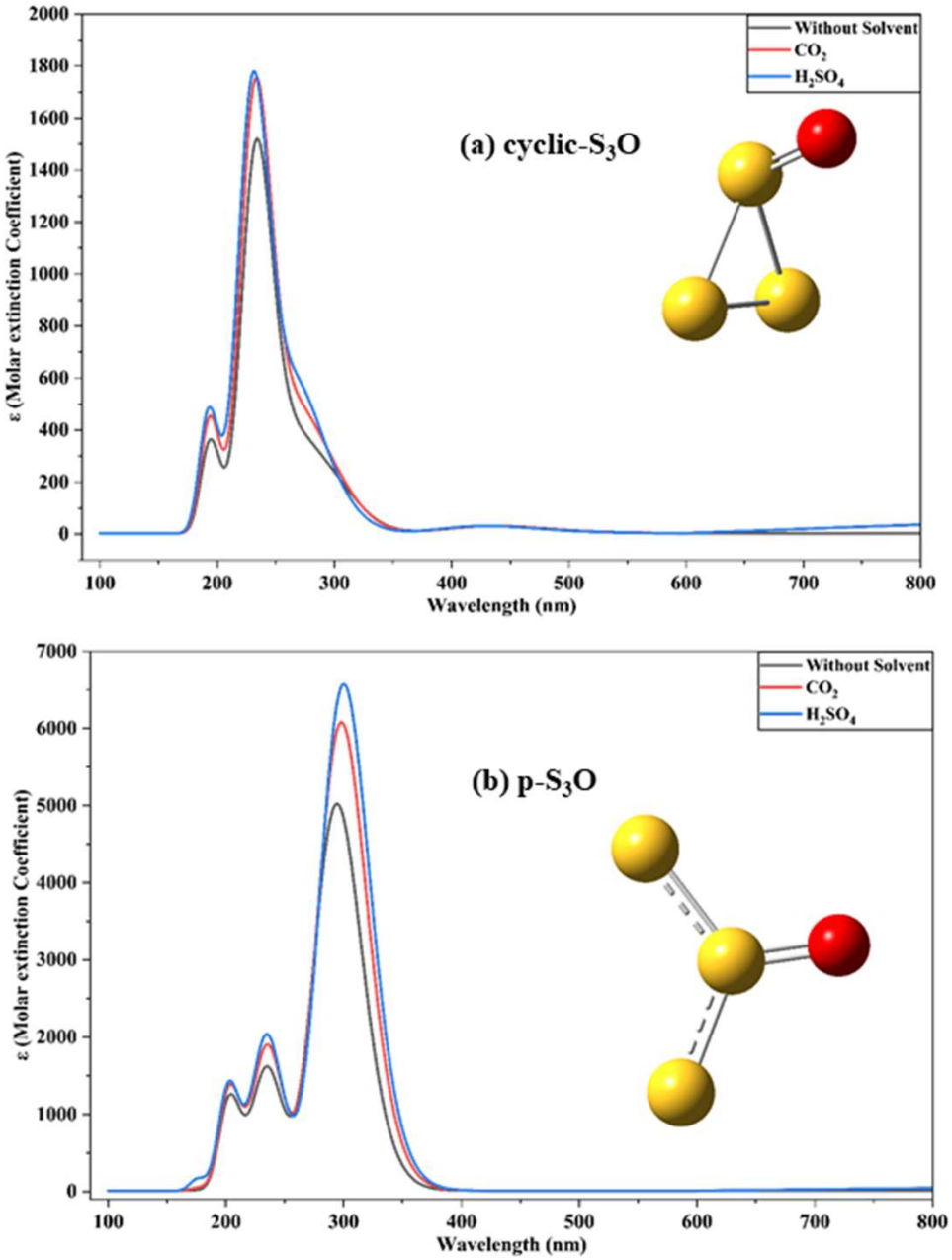

Figure 5. UV-Vis absorption spectrum of (**a**) cyclic and (**b**) planar isomers of S_3O, in three different environments, viz., gas phase (without solvent effects), CO_2 atmospheric medium, and H_2SO_4 aerosol phase using the SMD solvation model. Vertical excitation energies were calculated using Time-Dependent Density Functional Theory (TD-DFT) at the CAM-B3LYP/def2-TZVPP level. Color representations for atoms are red—oxygen and yellow—sulfur.

3.5.2. In CO_2 Solvent

When evaluating p-S_3O within the Solvation Model based on Density (SMD), the molecule exhibits a profound sensitivity in different dielectric environments. In the bulk supercritical CO_2 simulation, the primary UV peak undergoes a bathochromic (red) shift to 299.51 nm, accompanied by a significant hyperchromic effect, pushing the oscillator strength to 0.1391. Unlike the red-shifting of planar isomer, c-S_3O actively resists environmental stabilization. As the solvent polarity increases from vacuum to CO_2, the primary mid-UV

peak shifts backward to higher energies, from 231.57 nm (vacuum) to 230.19 nm, yielding a slight hypsochromic (blue) shift.

3.5.3. In H_2SO_4 Solvent

Within the highly polar H_2SO_4 solvent, the true potency of p-S_3O emerges as the bathochromic shift extends the peak to 301.26 nm. The transition probability climbs to a maximum of f = 0.1551, pushing the molar extinction coefficient beyond 6000 L mol^{-1} cm^{-1}. When p-S_3O absorbs a 301 nm photon, the electron density shifts drastically along the extended planar backbone, creating a highly polar excited state. The strong dielectric field of the surrounding H_2SO_4 molecules quickly aligns to stabilize this sudden dipole, effectively lowering the energetic barrier for the transition and vastly increasing the probability of photon capture. When cyclic-S_3O is solvated in sulfuric acid, the primary absorption manifold splinters into two weak transitions, blue-shifted peaks at 227.03 nm (f = 0.0195) and 236.08 nm (f = 0.0193). The visible trace feature shifts to 430.16 nm but remains utterly forbidden (f = 0.0007). This blue-shifting behavior confirms the "drumhead" correlation. In the cyclic geometry, the non-bonding electron pairs on the sulfur and oxygen atoms are forced into close, rigid proximity. The highly polar sulfuric acid environment stabilizes these concentrated ground-state electrons fiercely. Because the rigid ring prevents the molecule from reorganizing its geometry during excitation, the excited state cannot achieve the same solvent stabilization. This widens the HOMO-LUMO energy gap, forcing the molecule to require higher-energy, shorter-wavelength photons just to achieve excitation. Furthermore, the physical dimensions of the ring restrict the transition of the dipole moment. The charge cannot be displaced across a wide spatial distance, resulting in the heavily stunted oscillator strengths (f < 0.02).

The data firmly rule out cyclic-S_3O as a contributor to the Venusian optical profile. Its maximum oscillator strength in aerosol conditions (0.0195) is nearly eight times weaker than that of the planar isomer (0.1551). To generate the profound opacity observed in the Venusian clouds, c-S_3O would have to be present in staggering, thermodynamically impossible concentrations. Furthermore, its absorption is restricted to the deep 230 nm range, a region already entirely blacked out by the massive abundance of background sulfur dioxide (SO_2). In the context of atmospheric radiative transfer, cyclic-S_3O is a spectroscopic ghost. While p-S_3O is a remarkably efficient absorber, it does not match the 365 nm signature of the "unknown absorber." Its absorption firmly terminates at 301.26 nm in the H_2SO_4 phase. However, this specific wavelength positioning is critical. Solar radiation between 200 and 290 nm is heavily filtered by the uppermost SO_2 layers. Planar S_3O, sitting directly at 300 nm, acts as the immediate spectral successor to SO_2. We propose that p-S_3O functions as a mid-UV barrier, intercepting the 300–320 nm flux that manages to bypass the SO_2 shield, thus protecting the lower cloud layers from aggressive photolysis.

3.6. UV-Vis Spectral Characteristics of ClSSCl (Disulfur Dichloride) and $SSCl_2$ (Thiothionyl Chloride)

Having evaluated sulfur-oxygen species, our investigation must inevitably account for the presence of halogens in the Venusian atmosphere. Chlorine is a well-documented trace constituent, primarily existing as hydrogen chloride (HCl) below the cloud decks. However, photochemical models proposed by Krasnopolsky and others suggest that upward mixing of chlorine species into the sulfur-rich middle atmosphere should yield mixed sulfur-halogen compounds [23]. Disulfur dichloride (Gauche Isomer of S_2Cl_2) (ClSSCl) is a highly probable intermediate in these reaction networks [14]. By analyzing the TD-DFT spectral data of S_2Cl_2 across different solvent matrices, we aim to determine if this chlorinated species contributes to the near-UV opacity or if it functions strictly as a deep-atmosphere halogen reservoir (shown in Table 1 and Figure 6). To ensure a comprehensive

and balanced evaluation of the sulfur-chlorine parameter space, as dictated by thermodynamic accessibility and photochemical kinetics, we expanded our analysis to include the higher-energy branched isomer, thiothionyl chloride ($SSCl_2$). While thermodynamically less stable than the linear S_2Cl_2 isomer by approximately 12 kcal/mol, the steady-state radical recombination within the highly active Venusian cloud decks makes it a highly viable transient species. Our TD-DFT analysis reveals a spectral profile that is drastically different from its linear counterpart, introducing critical mid-UV opacity (Figure 6).

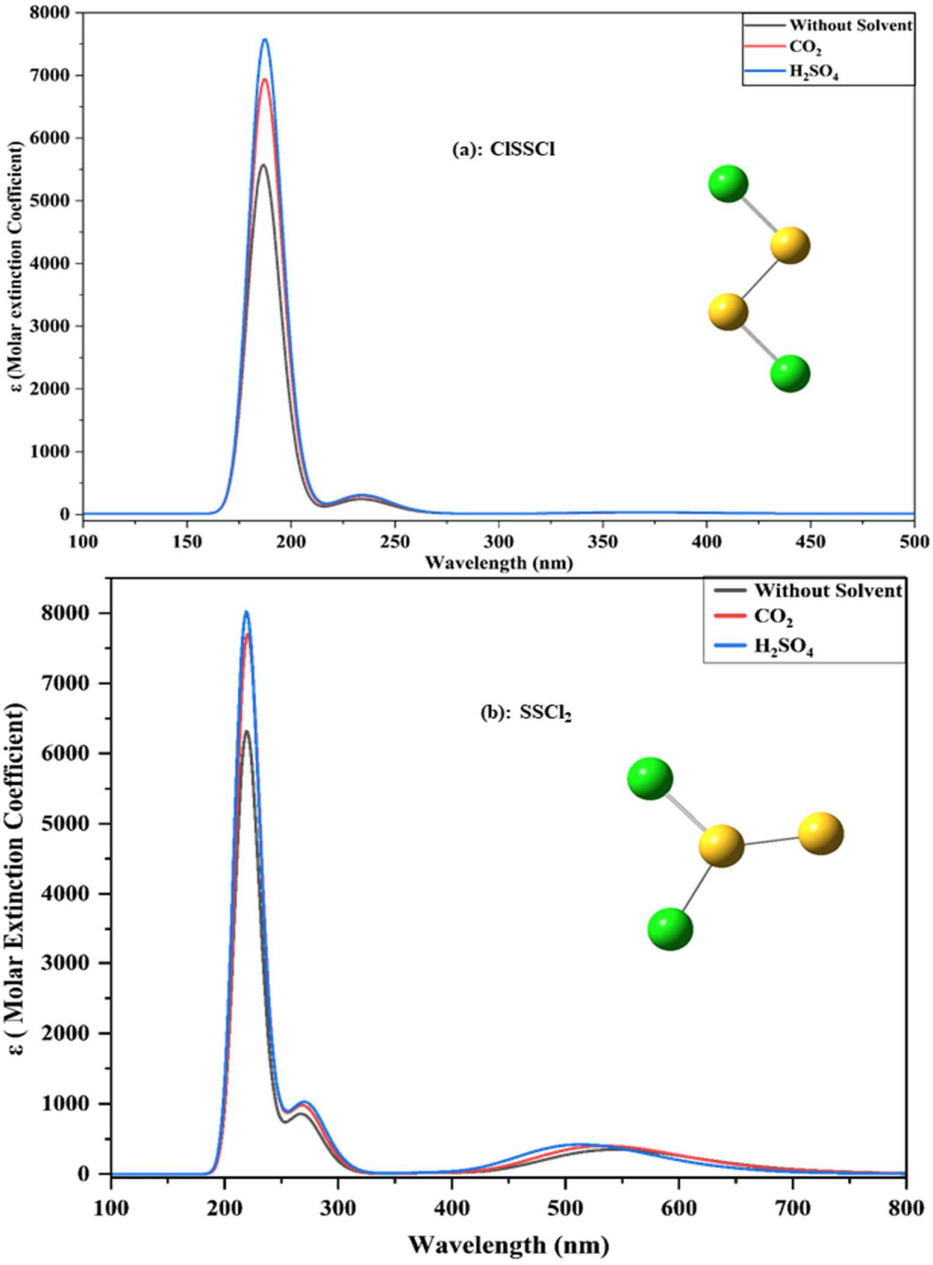

Figure 6. UV-Vis absorption spectrum of (**a**) ClSSCl and (**b**) $SSCl_2$ in three different environments, viz., gas phase (without solvent effects), CO_2 atmospheric medium, and H_2SO_4 aerosol phase using the SMD solvation model. Vertical excitation energies were calculated using Time-Dependent Density Functional Theory (TD-DFT) at the CAM-B3LYP/def2-TZVPP level. Color representations for atoms are green—chlorine and yellow—sulfur.

3.6.1. In Gas Phase (Without Solvent)

To establish the fundamental electronic properties of ClSSCl, we first examined its gas-phase UV-Vis spectrum. Unlike the highly conjugated or resonant structures of t-OSSO

and S_2O, sulfur monochloride adopts a twisted C_2 symmetry. Based on our calculated gas phase analysis, the dominant absorption feature is located deep in the vacuum-UV region at 186.83 nm. This transition possesses a high oscillator strength (f = 0.1376) and a massive molar extinction coefficient ($\varepsilon \approx 5500$ L mol^{-1} cm^{-1}). This high-energy peak is characteristic of an $\sigma \rightarrow \sigma^*$ transition localized on the S-Cl bonds, or an $n \rightarrow \sigma^*$ excitation originating from the chlorine lone pairs. Into the mid-UV, the spectrum reveals a very weak set of secondary transitions at 235.86 nm (f = 0.0047) and 226.55 nm (f = 0.0013). These likely represent symmetry-forbidden transitions or excitations from the sulfur non-bonding orbitals. The 370 nm feature possesses a practically negligible oscillator strength of f = 0.0005, indicating a highly forbidden electronic transition, likely a singlet-triplet excitation that only gains trace intensity via spin–orbit coupling induced by the heavy chlorine atoms. Unlike ClSSCl, which is defined by a massive vacuum-UV transition and near-UV transparency, the $SSCl_2$ geometry (featuring a terminal S=S bond) shifts the electronic activity toward lower energies. The gas-phase spectrum reveals a primary, highly intense absorption deeper in the UV at 219.51 nm (f = 0.1558). More crucially for atmospheric modeling, $SSCl_2$ exhibits a distinct mid-UV absorption band peaking at 268.30 nm with an oscillator strength of f = 0.0207. A weak, low-energy feature is also present in the visible region at 543.89 nm (f = 0.0086), characteristic of the branched thiosulfoxide geometry.

3.6.2. In CO_2 Solvent

When the background atmospheric condition, such as CO_2 solvent, was introduced as an implicit solvent, the spectral shifts were minimal but measurable. The primary VUV peak underwent a very slight bathochromic (red) shift from 186.83 nm to 187.50 nm. Interestingly, while the wavelength shift is negligible, the intensity of the absorption increases significantly, with the oscillator strength climbing from 0.1376 to 0.1715. This indicates that the induced dipoles in the surrounding CO_2 matrix effectively stabilize the transition dipole moment of the excited state of ClSSCl. The near-UV "dark state" remains fixed at 369.78 nm with an unchanged oscillator strength of f = 0.0005. For $SSCl_2$, the spectral features undergo a noticeable bathochromic (red) shift accompanied by hyperchromic enhancement. The primary vacuum-UV transition shifts slightly to 220.19 nm with a substantial increase in oscillator strength to f = 0.1891. The critical mid-UV band undergoes a red shift to 269.72 nm, with its transition probability climbing to f = 0.0235. This indicates that the induced dipoles in the surrounding CO_2 matrix effectively stabilize the transition dipole moment of the excited state of $SSCl_2$, enhancing its photon-capture efficiency in the planetary troposphere.

3.6.3. In H_2SO_4 Solvent

The electronic spectral analysis of ClSSCl within the highly polar sulfuric acid (solvent) droplets (H_2SO_4) amplifies the trends observed in the CO_2 model. The dominant VUV transition stabilizes at 187.59 nm. The most critical physical finding here is the continued hyperchromic effect. The oscillator strength for this transition maximizes at 0.1873. This intense hyperchromicity proves that the highly acidic and high-dielectric environment of the aerosols actively facilitates the absorption of high-energy photons by S_2Cl_2. However, the near-UV behavior remains stubbornly inactive. The peak at 367.30 nm shows an oscillator strength of only f = 0.0006. For the $SSCl_2$ isomer, the true atmospheric potency emerges within the highly polar and acidic H_2SO_4 aerosol simulation. The strong dielectric environment drives a further bathochromic shift in the mid-UV absorption band, stabilizing it at 271.84 nm. This shift is paired with a continued hyperchromic effect, pushing the oscillator strength to its maximum of f = 0.0244. Concurrently, the highest-energy transition stabilizes at 219.07 nm with a massive oscillator strength (f = 0.1958).

Based on our TD-DFT analysis, we can unambiguously eliminate sulfur monochloride (ClSSCl) as a candidate for the primary Venusian unknown absorber. Data obtained in this work outlined a vital role for this molecule in the altitude-dependent chemistry of Venus. Because ClSSCl is transparent to wavelengths above 250 nm, it is effectively immune to photolysis in the lower cloud layers (below 50 km), where shorter VUV wavelengths have already been filtered out by the upper atmosphere. This optical transparency guarantees extreme thermodynamic stability for ClSSCl in the deep atmosphere. It functions as a stable chemical reservoir, safely storing both sulfur and chlorine within the thick H_2SO_4 cloud droplets. However, the massive absorption peak at 187.59 nm dictates its ultimate fate. If vertical convection advects ClSSCl into the upper cloud decks (above 65 km), it will be abruptly exposed to unattenuated high-energy solar flux. The extreme oscillator strength in this region guarantees rapid and violent photolysis. The absorption of a 187 nm photon carries enough energy to cause immediate homolytic cleavage of the S-Cl and S-S bonds, instantly flooding the upper atmosphere with highly reactive atomic chlorine ($Cl^{\cdot}$) and sulfur radicals ($S^{\cdot}$ or $S_2^{\cdot}$). These generated halogen radicals are known to act as aggressive catalytic destructors. Chlorine radicals rapidly catalyze the oxidation of carbon monoxide (CO) back into carbon dioxide (CO_2), stabilizing the bulk atmosphere against continuous solar degradation. Furthermore, these radicals interact aggressively with the polysulfur (S_n) chains, potentially breaking down the actual near-UV absorbers (like t-OSSO or S_3) at high altitudes. The data obtained by TD-DFT analysis of $SSCl_2$ provides a vital contrast to the linear isomer. Unlike ClSSCl, which is entirely transparent beyond 250 nm, the $SSCl_2$ isomer acts as a potent, broadband mid-UV absorber. This stark isomeric contrast underscores the necessity of considering kinetically trapped, higher-energy species when modeling planetary opacity. The presence of $SSCl_2$ in the acidic aerosols would seamlessly bridge the absorption gap between the mid-UV (dominated by S_2O at ~276 nm) and the near-UV (dominated by t-OSSO at ~379 nm). While ClSSCl functions strictly as a deep-atmosphere halogen reservoir, the $SSCl_2$ isomer actively participates in the radiative balance of the middle cloud layers, continuously scavenging photons before they can penetrate deeper into the atmosphere.

3.7. UV-Vis Spectral Characteristics of $FeCl_3$

The inclusion of iron-bearing species in this work in the search for the Venusian "unknown absorber" is due to their known presence in the crust of the planet and potential lofting into the middle cloud layers (48–55 km). Specifically, iron(III) chloride ($FeCl_3$) has been considered a highly anticipated candidate. Unlike the main-group sulfur and chlorine species (t-OSSO, S_2Cl_2) analyzed previously, $FeCl_3$ is a transition metal complex. Its partially filled d-orbitals introduce entirely new electronic dynamics, including ligand-to-metal charge transfer (LMCT) and d-d transitions. However, our Time-Dependent Density Functional Theory (TD-DFT) analysis of $FeCl_3$ monomer generated profound wave function instabilities (negative roots indicating spin-symmetry breaking) and failed to locate any allowed transitions in the UV-visible range. The simulated data reveal significant computational and physical realities about modeling open-shell metal complexes in planetary atmospheres, ultimately challenging the hypothesis that monomeric $FeCl_3$ serves as the primary near-UV absorber (shown in Table 1 and Figure 7). Crucially, we present these findings as a valuable negative result to highlight the limitations of current modeling paradigms.

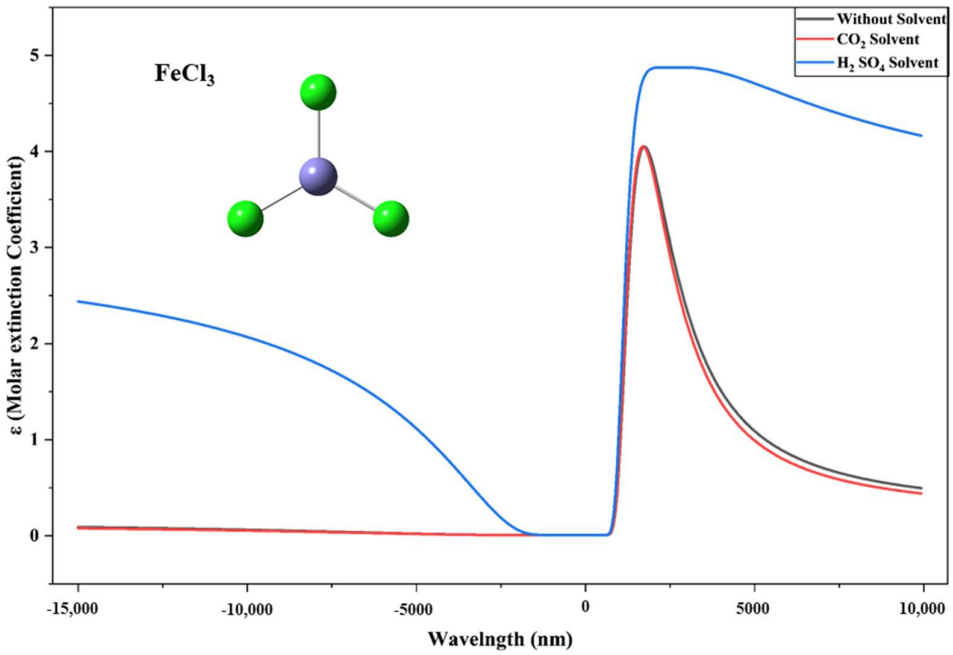

Figure 7. UV-Vis absorption spectrum of $FeCl_3$, in three different environments, viz., gas phase (without solvent effects), CO_2 atmospheric medium, and H_2SO_4 aerosol phase using the SMD solvation model. Vertical excitation energies were calculated using Time-Dependent Density Functional Theory (TD-DFT) at the CAM-B3LYP/def2-TZVPP level. Color representations for atoms are green—chlorine and blue—iron.

3.7.1. In Gas Phase (Without Solvent)

The initial gas-phase (vacuum) calculations of $FeCl_3$ present a highly unusual spectral output. The raw TD-DFT excitation data are dominated by a series of transitions with negative wavelengths. Specifically, the output identifies major roots at −1392.13 nm, −2275.78 nm, −2849.45 nm, −3701.68 nm, and extending down to −6407.17 nm. In the context of TD-DFT, a negative excitation energy is not a physically observable absorption event; rather, it is a mathematical piece indicating a wave function instability. High-spin Fe^+ is a d^5 system with five unpaired electrons. When subjected to certain hybrid functionals, the self-consistent field (SCF) ground state can become a saddle point on the potential energy surface rather than a true local minimum. This "triplet instability" (or spin-symmetry breaking) occurs because the functional struggles to properly correlate the highly localized, open-shell d-electrons, resulting in non-physical negative excitation roots. Looking past the instabilities to the physically observable (positive) roots, the gas-phase spectrum of $FeCl_3$ is devoid of any ultraviolet absorption. Instead, the calculated transitions appear deep in the near-infrared (NIR) and mid-infrared regions. The primary positive features are located at 9727.68 nm, 7854.54 nm, 6329.44 nm, and 1816.64 nm. The highest-energy transition in this simulated phase occurs at 1755.52 nm. Furthermore, the transition probability for this 1755.52 nm peak is exceptionally low, with a reported intensity value of just 0.0001. This minuscule extinction coefficient is a classic hallmark of Laporte-forbidden and spin-forbidden d-d transitions. Because the high-spin d^5 configuration of Fe^{3+} lacks any higher-energy empty d-orbitals of the same spin multiplicity, an electron must flip its spin to undergo a d-d transition (e.g., transitioning from a sextet ground state to a quartet excited state). The strict quantum mechanical selection rules prohibit these transitions, resulting in the near-zero intensity observed in our simulation.

3.7.2. In CO_2 Solvent

Embedding $FeCl_3$ in a simulated CO_2 environment does not resolve the open-shell wavefunction instabilities; negative roots persist extensively, reaching −6090.19 nm. However, the solvent field does induce a subtle hypsochromic (blue) shift in the observable infrared transitions. The primary NIR peak shifts from 1755.52 nm in a vacuum to 1715.75 nm under CO_2 solvation. Other accompanying low-energy states appear at 10,038.00 nm, 7197.49 nm, 7083.53 nm, and 1813.54 nm. Despite the slight blueshift, the intensity of the 1715.75 nm transition remains locked at a negligible value of 0.0001. The non-polar, weakly interacting CO_2 matrix lacks the necessary coordination chemistry to break the Laporte selection rules or significantly alter the spin state of the iron center.

3.7.3. In H_2SO_4 Solvent

When induced in the highly polar, acidic environment of the H_2SO_4 solvent, the most significant distortion of the $FeCl_3$ electronic structure occurs. The negative instability roots are slightly compressed, terminating at −5344.10 nm. More importantly, the high-dielectric medium drastically shifts the positive absorption manifold. A new, extremely low-energy state emerges at 13,907.99 nm and 13,877.84 nm. The mid-IR transitions split, yielding a feature at 5979.32 nm with an intensity of 0.0001. The highest-energy observable transition is further blue-shifted to 1594.30 nm, while maintaining its forbidden intensity character (0.0001). This progressive blueshift in the highest-energy d-d transition (from 1755 nm in vacuum to 1594 nm in H_2SO_4) indicates an increase in the ligand field splitting energy. The strong dielectric screening of sulfuric acid effectively acts as a stronger field environment around the $FeCl_3$ monomer, pushing the excited d-states to slightly higher energies. However, even with this environmental forcing, the transitions remain firmly trapped in the infrared spectrum.

The computational model of this study identifies absolutely zero electronic transitions in the ultraviolet or visible regions. The highest energy absorption recorded across all solvent models is 1594.30 nm. Based on this specific electronic configuration, monomeric $FeCl_3$ is entirely transparent to the near-UV radiation that characterizes the Venusian albedo drop. Even if vibrational coupling or temperature effects broadened the infrared peaks, their transition probabilities are too low to matter. An intensity value of 0.0001 is orders of magnitude weaker than the allowed $\pi \rightarrow \pi^*$ transitions seen in candidates like t-OSSO. Generating the observed planetary opacity with such forbidden transitions would require an atmosphere composed almost entirely of $FeCl_3$, which violently contradicts mass spectrometry data from the Pioneer Venus and Venera descent probes. Experimental laboratory spectra of bulk, solvated $FeCl_3$ often exhibit an intense, broad absorption in the 300–400 nm range. This divergence between our computational data and available literature is due to the limitations of the computational methodology when applied to specific chemical models. The strong UV absorption seen in experimental $FeCl_3$ is not a d-d transition; it is a Ligand-to-Metal Charge Transfer (LMCT) band, where an electron from the chlorine p-orbitals is photo-excited directly into the empty iron d-orbitals. Standard TD-DFT, particularly when employing range-separated functionals designed to cure self-interaction error in organic molecules, often drastically overestimates the energy required for LMCT transitions in transition metals. It is highly probable that the computational protocol has pushed the theoretical LMCT band of $FeCl_3$ deep into the vacuum-UV (e.g., <100 nm), leaving only the forbidden and low-energy d-d transitions. Furthermore, our theoretical work evaluates an isolated $FeCl_3$ monomer surrounded by an implicit solvent field. In the actual Venusian aerosols, Fe^{3+} would likely undergo explicit solvolysis, forming complex ionic species like $[Fe(SO_4)_2]^-$ or $[FeCl_4]^-$. The direct covalent coordination of oxygen from the sulfuric acid to the iron center would fundamentally rewrite the molecular orbital

diagram, likely pulling strong LMCT bands back into the near-UV range as observed in bulk experimental studies. Therefore, while our implicit solvation models firmly disqualify the isolated $FeCl_3$ monomer as a contributor to the planetary opacity, a definitive evaluation of iron's atmospheric role necessitates future models that incorporate explicit aerosol coordination domains.

3.8. UV-Vis Spectral Analysis of Phosphine (PH_3)

The detection of phosphine (PH_3) in the Venusian cloud decks has invited one of the most intense debates in contemporary planetary science [52,53]. While much of the discourse centers on its potential as a bio signature or the result of unknown abiotic reductive chemistry, our focus in this study was its immediate photophysical behavior, whether PH_3 actively contributes to the anomalous ultraviolet opacity of Venus, or is it a fleeting, transparent bystander. To answer this, we subjected PH_3 to our Time-Dependent Density Functional Theory (TD-DFT) protocol. Phosphine is a pyramidal molecule defined by a highly polarizable non-bonding electron pair on the central phosphorus atom. The spectral data reveal that this lone pair acts as a highly sensitive environmental probe. By tracking its electronic transitions across different dielectric models, we observe a profound demonstration of ground-state stabilization and excited-state hyperchromic, ultimately ruling out PH_3 as the visible-light or near-UV planetary absorber, while confirming its status as a highly vulnerable photochemical precursor. (Shown in Table 1 and Figure 8).

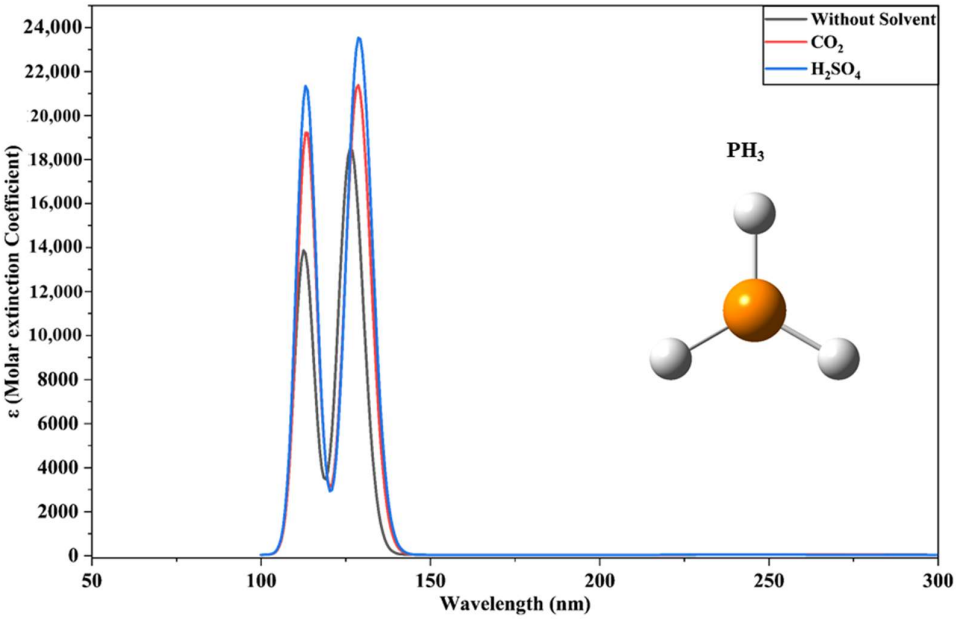

Figure 8. UV-Vis absorption spectrum of PH_3, in three different environments, viz., gas phase (without solvent effects), CO_2 atmospheric medium, and H_2SO_4 aerosol phase using the SMD solvation model. Vertical excitation energies were calculated using Time-Dependent Density Functional Theory (TD-DFT) at the CAM-B3LYP/def2-TZVPP level. Color representations for atoms are white—hydrogen and orange—phosphorus.

3.8.1. In Gas Phase (Without Solvent)

We established the baseline electronic signature of phosphine in a gas phase without any solvent, where the molecule is free from external dielectric screening. The resulting gas-phase spectrum is characterized by extreme optical transparency in the near-UV and visible regions, paired with a massive absorption cross-section in the deep vacuum-ultraviolet (VUV). The near/mid-UV region contains a single, highly forbidden transition located at 258.43 nm. The probability of this transition occurring is near zero, evidenced by a

minuscule oscillator strength of f = 0.0003 and a molar extinction coefficient of roughly 235 L mol^{-1} cm^{-1}. This peak likely represents an excitation from the phosphorus lone pair (n) into a highly localized, anti-bonding σ* orbital. The poor spatial overlap between these specific orbitals dictates the low transition probability. We also observed a high absorption feature at 126.56 nm, imposing an oscillator strength of f = 0.4574 and an extinction coefficient exceeding 18,000 L mol^{-1} cm^{-1}. A secondary, weaker high-energy transition is also present at 112.80 nm (f = 0.1693). These deep VUV features are characteristic of Rydberg transitions. When interacted with a high-energy photon, an electron from the phosphorus lone pair is ejected into a diffuse, large-radius Rydberg orbital (n → 4s or n → 4p). Because these Rydberg orbitals physically encompass the entire molecule, the transition dipole moment is massive, resulting in the overwhelming intensity observed at 126.56 nm.

3.8.2. In CO_2 and H_2SO_4 Solvent

The TD-DFT analysis of PH_3 in CO_2 and H_2SO_4 solvation suggested that the transition from a vacuum to the dense Venusian cloud layers drastically alters the electronic landscape of phosphine. In the supercritical CO_2 solvation, the weak mid-UV peak experiences a hypsochromic (blue) shift, migrating from 258.43 nm down to 251.61 nm. The transition probability simultaneously decays to f = 0.0002. This suppression is aggressively magnified in the simulated H_2SO_4 aerosol matrix. The peak is violently blue-shifted to 237.61 nm, and its oscillator strength drops to an absolute trace level of f = 0.0001, reducing its extinction coefficient to just 69.6 L mol^{-1} cm^{-1}. This 20 nm blueshift was rooted entirely in the chemical nature of the sulfuric acid droplet. The non-bonding lone pair on the phosphorus atom is highly nucleophilic and prone to hydrogen-bonding interactions. In a highly acidic, high-dielectric environment like H_2SO_4, the solvent shell rigidly coordinates around that lone pair. This aggressive solvation fundamentally stabilized the ground state of the PH_3 molecule, pulling its energy level down into a deep thermodynamic well, effectively mimicking the early stages of protonation to form a phosphonium (PH_4^+) geometry [52]. Because the ground state is anchored so deeply by the solvent, the energy gap to the unsolvated σ* excited state widens considerably. The molecule, therefore, demands a much higher energy photon (shorter wavelength) to force the electron out of its comfortable solvent cage, pushing the absorption peak from 258 nm deep into the 237 nm region. While the acidic solvent suppresses the low-energy transitions, it actively amplifies the high-energy Rydberg states. We observed a pronounced bathochromic (red) shift coupled with extreme hyperchromicity (intensity enhancement) in the VUV region. In the CO_2 matrix, the primary 126.56 nm peak shifts to 128.67 nm, while its oscillator strength leaps from 0.4574 to 0.5279. The secondary peak also shifts red to 113.54 nm (f = 0.2358). The H_2SO_4 environment pushes this trend to its absolute limit. The primary VUV transition stabilizes at 129.04 nm, but its oscillator strength rockets to f = 0.5819. The secondary peak mirrors this behavior, shifting to 113.40 nm with an elevated intensity of f = 0.2619. The high-energy peak shifts red while the low-energy peak shifts blue, which is due to the polarizability of the excited state. A Rydberg excited state is highly diffuse; the electron cloud expands significantly away from the central atomic nuclei. The high dielectric constant of the sulfuric acid matrix is exceptionally efficient at stabilizing large, diffuse charge distributions. Therefore, the solvent stabilized the expanded excited state much more effectively than it stabilizes the ground state, shrinking the overall energy gap and shifting the peak to a longer wavelength. Simultaneously, the surrounding solvent molecules constructively interacted with the expanding transition dipole moment. This structural coupling allows the PH_3 molecule to capture incoming photons with good efficiency, resulting in the massive 27% increase in oscillator strength compared to the vacuum baseline.

When we mapped these rigorous quantum chemical results onto the macroscopic reality of the Venusian atmosphere, we generated a definitive framework for the role of phosphine. First, PH_3 is unequivocally disqualified as the source of the 365 nm unknown absorber phenomenon. Across all evaluated dielectric models—from a pure vacuum to supercritical CO_2 to concentrated sulfuric acid, phosphine lacks a single electronic transition above 260 nm. It is entirely transparent to near-UV, blue, and visible light. The molecule cannot physically absorb the wavelengths necessary to create the dark, contrast-heavy cloud markings seen by the Pioneer Venus or Akatsuki orbiters. However, its transparency in the near-UV is contrasted by its absolute opacity in the deep VUV. An oscillator strength of f = 0.5819 at 129.04 nm within the aerosol phase indicates that PH_3 is a terminal photon sink for high-energy solar flux. The energy carried by a 129 nm photon is massive (nearly 9.6 eV), far exceeding the bond dissociation energy of the phosphorus-hydrogen bond (~3.3 eV). Consequently, the moment a PH_3 molecule absorbs a photon in this primary band, it will undergo instantaneous photolysis. The transition will violently eject a hydrogen atom, generating the highly reactive PH_2 radical. This dictates a harsh astrochemical reality that phosphine cannot survive in the upper cloud decks. Its colossal absorption cross-section ensures that it will be rapidly dismantled by ambient Lyman-alpha and deep VUV solar radiation at high altitudes. The presence of PH_3 on Venus must therefore be confined to the deep, optically thick lower atmosphere or the surface, where the overlying carbon dioxide and sulfur dioxide layers act as a physical shield against the 129 nm radiation it so avidly absorbs. Any phosphine actively lofted into the middle and upper clouds will not contribute to the planet's visible albedo; instead, it will be instantly shredded by the sun, feeding a complex, localized cascade of radical phosphorus chemistry that eventually oxidizes into stable phosphoric acid (H_3PO_4) derivatives.

4. Spectroscopic Analysis of the Venusian Atmospheric Chromophores

4.1. Assessment of Contribution to the Unknown UV Absorber

The upper cloud decks of Venus, extending from 60 to 70 km in altitude, exhibit a massive, broad optical absorption that dramatically reduces the planetary albedo between 320 and 400 nm, with a maximum near 365 nm. This phenomenon is responsible for absorbing nearly half of the solar energy deposited into the Venusian atmosphere, driving the aggressive super-rotation of the atmospheric column [27,51]. Using Time-Dependent Density Functional Theory (TD-DFT) utilizing the CAM-B3LYP functional, supplemented by the Solvation Model based on Density (SMD) [20,25] for the environment CO_2 and H_2SO_4 dielectrics, we systematically evaluated electronic transitions of proposed chemical candidates. Crucially, the identification of these chromophores must account for the vertical distribution of the absorbing material. While orbital imagers primarily capture the high-contrast features at the cloud tops (65–70 km), in situ measurements from the VeGa 1 and VeGa 2 descent probes demonstrate that the UV-absorbing substance is present across the entire cloud deck, extending deep into the lower clouds [54]. Because the majority of destructive, high-energy solar UV is absorbed by approximately 60 km, the environment in the middle and lower clouds is optically shielded. This deep-atmosphere reality validates the application of our H_2SO_4 aerosol solvation models. Below the cloud tops, species like OSSO and S_3O are not only heavily solvated by concentrated acidic droplets—which we have shown tunes their absorption properly to the observed wavelengths, but they are also protected from rapid photolysis, allowing them to accumulate and govern the radiative balance across a much thicker vertical column than cloud-top models alone suggest. Of all the species evaluated in this study, trans-OSSO (t-OSSO) appeared as the most physically robust match for the 365 nm Venusian signature. In the simulated sulfuric acid solvent matrix (H_2SO_4), t-OSSO undergoes a structural stabilization that

yields a primary absorption band at 379.37 nm with an oscillator strength of f = 0.1140. Rather than relying on historical gas-phase approximations, our solvated data prove that the macroscopic dielectric response of the acidic aerosol directly tunes the highly allowed $\pi \rightarrow \pi$ transition of t-OSSO to align perfectly with planetary albedo measurements. Furthermore, by applying the benchmarked validation data established in Section 2.1, this solvated peak provides an exceptional functional fit for the broad planetary albedo drop. Equally critical to the atmospheric energy budget are the optical properties of the polysulfur oxides and halogens, which our calculations explicitly quantify. Our TD-DFT data reveals that adding a single sulfur atom to the chain fundamentally shifts the absorption out of the UV and into the visible spectrum. Solvated cis-S_3O absorbs heavily at 436.31 nm (f = 0.1280), precisely filtering blue light required to produce the planet's characteristic yellow hue. Furthermore, our evaluation of the branched $SSCl_2$ isomer demonstrates that transient halogenated species are active radiative participants. $SSCl_2$ generates potent broadband near-UV opacity in H_2SO_4 (λ = 271.84 nm, f = 0.0244) that the linear S_2Cl_2 isomer fundamentally lacks. This isomeric contrast underscores the necessity of evaluating kinetically trapped, higher-energy species when modeling planetary opacity. Disulfur monoxide (S_2O) exhibits a considerable absorption peak at 276.93 nm (f = 0.1028) in H_2SO_4 aerosol conditions. While too energetic to be the unknown absorber, it acts as a critical mid-UV shield, effectively scavenging photons in the environment where background SO_2 absorption weakens. Similarly, the hydroxysulfonyl radical (HSO_3) absorbs at 338.70 nm in H_2SO_4; however, its transition is strictly forbidden (f = 0.0177), meaning it requires unrealistic column densities to generate the observed opacity. Planar S_3O proves to be a formidable absorber at 301.26 nm (f = 0.1551), serving as another mid-UV shield rather than the visible or near-UV contrast agent, while Cyclic S_3O (c-S_3O) completely fails to absorb beyond 236 nm, heavily constrained by its rigid ring topology (f < 0.02). Most notably, iron(III) chloride ($FeCl_3$) fails the criteria entirely as an isolated monomer. Our TD-DFT analysis uncovered severe wavefunction instabilities (negative roots) and revealed that uncoordinated $FeCl_3$ only undergoes highly forbidden, spin-restricted d-d transitions deep in the infrared (~1594 nm, f = 0.0001). This data provides a vital negative result: implicit continuum models are insufficient for modeling transition metal aerosols [22]. To capture the intense Ligand-to-Metal Charge Transfer (LMCT) bands observed in experimental data, iron must undergo explicit covalent coordination with the H_2SO_4 matrix, a phenomenon the SMD model cannot replicate for discrete monomers.

The viability of an atmospheric absorber is not solely dictated by its spectral match, but it must also physically survive long enough within the Venusian environment to exert a climatic effect. The calculated high-energy (vacuum-ultraviolet) absorption bands for these molecules provide a direct blueprint for their atmospheric destruction and reactivity. Our calculated high-energy absorption bands dictate absolute photochemical limits. The deep-VUV absorption of S_2Cl_2 at 187.59 nm possesses an extreme oscillator strength (f = 0.1873). Any S_2Cl_2 lofted to the cloud tops will undergo instantaneous homolytic cleavage, proving it functions exclusively as a deep-atmosphere halogen reservoir rather than a stable high-altitude absorber. Consequently, S_2Cl_2 cannot possess a long atmospheric lifetime at the cloud tops (65–70 km). Instead, it acts as a highly volatile photochemical precursor, violently dissociating to release chlorine radicals ($Cl^{\cdot}$) and sulfur monochloride radicals ($SCl^{\cdot}$). These radicals act as a catalyst, attacking background SO_2 and OCS to propagate the formation of longer polysulfur chains (S_n) [55]. Similarly, S_2O absorbs powerfully in the 276 nm region. Because the S-S bond dissociation energy is relatively low (~4.4 eV), photon capture at 276 nm (~4.5 eV) straddles the energetic threshold for photolysis. S_2O likely exists in a rapid, dynamic steady state, constantly destroyed by mid-UV flux to yield SO and S radicals, and constantly reformed by the recombination of those same fragments. The

photostability of the longer sulfur chains (S_2O_2 and S_3O) depends heavily on their structural geometry. The data show that the linear, conjugated chains (t-OSSO, p-S_3O) possess lower ground-state energies and highly allowed transition dipole moments compared to their cyclic or strained counterparts. When t-OSSO absorbs a 379 nm photon, the energy is delocalized across the π network. Rather than instantly fragmenting the molecule, this excitation often results in non-radiative decay or transient photoisomerization into c-OSSO. This reversible stereochemical flipping allows the OSSO system to function as an energy sponge. It absorbs destructive UV energy, harmlessly dissipates it via internal molecular rotation, and relaxes back to the ground state. This mechanism grants the OSSO isomers a significantly longer photochemical half-life in the upper clouds than reactive species like HSO_3 or S_2Cl_2. Furthermore, the extreme blueshift in HSO_3 in sulfuric acid (from 348 nm down to 338 nm) indicates strong hydrogen-bonding stabilization. While HSO_3 is generally considered a highly reactive radical intermediate in the oxidation of SO_2 to H_2SO_4, its ground-state stabilization by the aerosol droplets essentially traps it, protecting it from lower-energy photolysis and potentially allowing it to accumulate at the cloud bases (48–55 km) where UV flux is attenuated.

Venus maintains its extraordinary climatic super-rotation because a massive amount of solar energy is deposited directly into the middle atmosphere rather than reaching the planetary surface [27,56]. The identification of these multiple chromophores allows us to map the complete radiative balance of the Venusian cloud deck as a continuum of absorption. Based strictly on our TD-DFT calculations, we propose a multi-chromophore model where atmospheric opacity is generated by a chemically stratified layer of interconnecting absorption bands, intrinsically tuned by the acidic aerosol matrix. t-OSSO and $SSCl_2$ dominate the near-UV sink, S_2O and p-S_3O intercept mid-UV flux, and c-S_3O governs visible-light absorption, collectively sustaining the global atmospheric super-rotation. A single molecule simply cannot possess a transition dipole moment broad enough to cover 200 nanometers of the electromagnetic spectrum without resolving into sharp, discrete peaks. By utilizing an entire family of sulfur-oxygen chains, in which each is tuned to a specific wavelength by its unique orbital topology and solvatochromic interaction with the acidic aerosol, the Venusian atmosphere creates a seamless optical wall.

4.2. Atmospheric Formation Pathways and Chemical Viability

To robustly assess a molecule's suitability as a candidate UV absorber, its spectroscopic profile must be contextualized within the chemical realities of the Venusian atmosphere. The cloud decks (48–70 km) host a highly active sulfur photochemical cycle, fundamentally driven by the ultraviolet photolysis of SO_2 into SO and atomic oxygen, which cascade into a complex network of recombination reactions [18,55]. Within this established framework, several of the species modeled in our calculations emerge naturally as transient intermediates. For instance, the thiosulfeno isomers (S_2O_2) are chemically plausible products of sulfur monoxide radical recombination (SO + SO + M $\rightarrow$ OSSO + M) or the direct oxidation of diatomic sulfur (S_2 + O_2 $\rightarrow$ OSSO) [11]. Likewise, chain propagation involving S_2 and SO radicals offers a direct synthetic route to polysulfur oxides such as S_3O. The hydroxysulfonyl radical (HSO_3) is a well-documented intermediate formed via the gas-phase reaction of SO_2 with hydroxyl radicals (SO_2 + OH $\rightarrow$ HSO_3). Despite these viable formation pathways, evaluating OSSO and S_3O as a primary candidate requires addressing strict photochemical abundance constraints. Recent global photochemical models have argued against OSSO as the sole unknown absorber, predicting that its steady-state abundance at the uppermost cloud tops is severely depleted by rapid photolysis [57,58]. However, our quantum chemical data provides a necessary counterweight to this mass-abundance limitation. Because the primary $\pi \rightarrow \pi^*$ transition of solvated t-OSSO is exceptionally

allowed (possessing an oscillator strength of f = 0.1140 and a molar extinction coefficient exceeding 4680 L mol^{-1} cm^{-1}), it acts as a hyper-efficient pigment. Therefore, massive column densities are not strictly required; even trace, parts-per-billion (ppb) concentrations of t-OSSO maintained in a dynamic steady-state (via continuous SO recombination) can generate substantial macroscopic optical depth. Furthermore, as confirmed previously by the VeGa 1/2 descent profiles, its abundance is likely much higher in the shielded middle clouds, where it is protected from the unattenuated solar flux that drives its destruction at the cloud tops.

5. Vibronic Broadening, Photometric Viability, and Candidate Limitations

As highlighted by the vertical excitation data, local solvation models (bulk CO_2 and H_2SO_4 aerosols) produce relatively minor solvatochromic shifts (~2 to 10 nm). To accurately assess whether these candidate molecules can sustain the massive, order-of-magnitude larger shifts required to explain the Venusian >400 nm albedo drop, 1D vibronic sweep analysis was performed (detailed results are provided in Supplementary Table S2 and Figures S1 and S2).

The comparative photodynamics expose a distinct structural prerequisite for visible light absorption. The highly fluxional chains, specifically cis and trans-OSSO, exhibit a unique orbital topology. As their S–S and S–O bonds undergo physical elongation, the excitation energies red-shift severely into the visible and near-IR regions (trans-OSSO shifting to 638 nm) while remarkably maintaining robust oscillator strengths (f > 0.10). Interestingly, the isomeric fluxional chains, trans- and cis-S_3O, act as intermediate photometric contributors. In their ground states, they possess strong vertical transitions perfectly anchored at the violet/blue edge (498.62 nm, f = 0.1047 for trans-S_3O). However, unlike the resilient OSSO backbone, their transition probabilities decay rapidly upon structural elongation (dropping by >60 at a -0.20 Å displacement). Consequently, while these unbranched S_3O chains may strongly contribute to the initial >400 nm opacity boundary, they lack the electronic capacity to independently sustain the deep visible continuum tail.

In stark contrast, structurally constrained or purely dissociative control species fail to maintain photometric viability. When cyclic-S_3O and planar-S_3O or the OS_2 fragment undergo analogous structural elongation to capture longer wavelengths, their transition probabilities undergo a total collapse (f < 0.02). Similarly, the S_2Cl_2 control remains optically dark in the visible regime regardless of bond distortion. This confirms that broad vibronic tailing is not a universal trait of sulfur species; it strictly requires the unconstrained fluxionality of the OSSO backbone to sustain intense charge-transfer transitions deep into the visible spectrum. Because this intrinsic gas-phase vibronic broadening produces spectral shifts (hundreds of nanometers) that vastly overshadow the minor solvatochromic shifts (2–10 nm) induced by bulk CO_2 or H_2SO_4 aerosols, we can reasonably extrapolate that this fluxional broadening mechanism remains the dominant photometric driver across all Venusian solvation environments, satisfying the primary constraints of the unknown absorber.

To ensure a rigorous and unified mechanistic comparison, it was imperative to define the photophysical boundaries of this study. While the OSSO backbone demonstrates the unique capacity to sustain visible absorption, several historically proposed alternative candidates were systematically evaluated and subsequently excluded from the primary visible-absorption model due to fundamental quantum mechanical limitations. Although HSO_3 is a critical open-shell intermediate in Venusian atmospheric chemistry, vertical TD-DFT screening reveals that its low-lying electronic states are non-viable as primary visible absorbers. The lowest energy transition occurs near the violet border (389.57 nm); however, this transition is symmetrically forbidden, possessing a negligible oscillator strength (f = 0.0002). Its brightest UV transitions (f ≈ 0.019 at 254 nm) remain an order

of magnitude weaker than those of the OSSO species. Because the radical possesses no bright states in the relevant optical window, dedicating exhaustive computational resources to vibronic broadening on its complex, open-shell potential energy surface was deemed photometrically irrelevant.

To test whether the continuum absorption tail is a generic feature of any fluxional sulfur-halogen chain, linear disulfur dichloride (S_2Cl_2) was subjected to the identical 1D Reflection Principle sweep. The data (Table S2) definitely prove that substituting oxygen for chlorine nullifies the effect. The primary bright states of S_2Cl_2 ($f > 0.50$) remain heavily trapped in the vacuum-UV (~160–180 nm). Even under extreme bond elongation (+0.40 Å), the red-shift stalls near 302 nm, and any states forced into the visible region become optically dark ($f = 0.0004$). Consequently, we explicitly excluded its branched isomer, thiothionyl chloride ($SSCl_2$), from vibronic mapping. Because structural rigidity fundamentally suppresses vibronic red-shifting, the highly constrained, branched geometry of $SSCl_2$ renders it photometrically inferior to the already non-viable linear S_2Cl_2 chain.

Despite recent interest in Venusian phosphine, its electronic structure lacks the requisite low-lying excited states necessary to contribute to the near-UV/visible absorption anomaly. PH_3 is highly transparent in the >400 nm regime, inherently disqualifying it as the primary unknown absorber. While $FeCl_3$ remains a proposed candidate in legacy literature, its absorption mechanism relies on transition-metal Ligand-to-Metal Charge Transfer (LMCT). The physics of LMCT are fundamentally distinct from the main-group $\pi \rightarrow \pi^*$ and $n \rightarrow \pi^*$ charge transfers governing the polysulfur oxides. Accurately modeling $FeCl_3$ requires entirely different methodological benchmarking, including relativistic Effective Core Potentials (ECPs) and multi-reference functional adjustments, placing it outside the comparative scope of this unified sulfur-oxygen mechanistic study.

6. Conclusions

The identification of the Venusian atmospheric absorbers requires models that account for exact solvatochromic behavior within the sulfuric acid cloud decks. The quantum chemical analysis executed in this study systematically dismantles the single-molecule absorber hypothesis and demonstrates that the optical anomalies of the Venusian atmosphere must be modeled not as a collection of isolated gases, but as a complex, highly dynamic, solvated chemical network. By systematically benchmarking the CAM-B3LYP functional against high-level EOM-CCSD and MRCI+Q wave function references, the calculated oscillator strengths and excitation energies deployed in this study are proven to be highly robust for extended sulfur-halogen systems. The solvent-induced stabilization is the fundamental physical mechanism that forces the massive hyperchromic enhancements and distinct solvatochromic shifts responsible for aligning these species with the observed planetary albedo.

From this study, we established a unified multi-chromophore framework governed by the following phase-dependent spectral behaviors:

- Near-UV Absorbers: t-OSSO dominates the 365 nm unknown absorber window via a highly allowed, bathochromically shifted $\pi \rightarrow \pi^*$ transition in the aerosol phase (379.37 nm, $f = 0.1140$). This primary absorption is supported by the kinetically trapped thiothionyl chloride ($SSCl_2$) isomer, which introduces a highly stable, broadband absorber, seamlessly bridging the gap between sulfur opacity and halogen radical chemistry.
- Visible-Light Absorbers: Our solvated calculations confirm that the addition of a single sulfur atom shifts the primary absorption into the visible spectrum. Solvated cis-S_3O absorbs heavily at 436.31 nm ($f = 0.1280$), effectively filtering the blue light required to produce the planet's characteristic yellow hue.

- Mid-UV Shields and Deep-UV Reservoirs: Disulfur monoxide (S_2O) and planar-S_3O exhibit intense mid-UV absorption (276.93 nm and 301.26 nm, respectively), acting as highly efficient photolytic shields in the lower clouds. Conversely, linear S_2Cl_2 is entirely transparent in the near-UV but possesses a massive, hyperchromic vacuum-UV transition (187.59 nm, f = 0.1873) that guarantees rapid photolysis if lofted above the cloud tops.
- The Transition Metal Constraint: The failure of implicit continuum modeling to locate any allowed UV-visible transitions for monomeric $FeCl_3$ (yielding only forbidden d-d transitions near 1594 nm) provides a critical computational boundary. To generate the intense LMCT bands observed experimentally, transition metals must undergo explicit covalent solvolysis with the H_2SO_4 matrix.
- By deploying a semi-classical Reflection Principle approach to map dissociative excited-state potentials, we demonstrated that standard harmonic Franck-Condon models fail to capture the photophysics of polysulfur oxides. Instead, the continuous absorption tail is driven by the extreme ground-state fluxionality of the OSSO backbone. While control species (such as S_2Cl_2, OS_2, and cyclic isomers) suffer a complete collapse of transition probability upon structural elongation, the unconstrained cis- and trans-OSSO chains maintain intense, symmetry-allowed charge-transfer transitions deep into the visible spectrum (>600 nm). This uniquely isolates the fluxional OSSO motif as the requisite structural driver for the Venusian unknown UV-visible absorber.

The Venusian clouds operate as a planetary-scale chemical reactor, where the acidic solvent matrix is the indispensable catalyst allowing a stratified network of open-chain sulfur and chlorine species to capture the vast quantities of solar energy required to sustain a global atmospheric super-rotation. We emphasize that the present study focuses strictly on the intrinsic spectroscopic properties and solvatochromic behaviors of the suggested candidate molecules. Deriving precise steady-state atmospheric concentrations requires comprehensive 3D photochemical and atmospheric transport modeling, which falls beyond the scope of this work. Nevertheless, by identifying specific isomers whose electronic transitions strongly coincide with the Venusian UV-visible absorption window, these calculations establish vital theoretical constraints. Integrating this quantum chemical data with global photochemical models will ultimately clarify the precise contribution of these species to the planetary albedo.

Supplementary Materials: The following supporting information can be downloaded at: https://www.mdpi.com/article/10.3390/universe12050151/s1, Figure S1: Simulated 1D Vibronic Absorption Envelopes of the S_xO_y Candidate Pool. Plotted on an absolute intensity scale, this overlay demonstrates the massive photometric superiority of the fluxional OSSO chains in the >400 nm region compared to the isomeric S3O analogues; Figure S2: Auto-scaled individual vibronic envelopes for each candidate and control species. While the absolute intensities of the rigid and control species are photometrically negligible in the visible region, these auto-scaled plots highlight the distinct vacuum-UV and near-UV localized transition peaks prior to structural elongation; Table S1: Cartesian coordinates at M06-2X/def2-ZVPP Level of Theory; Table S2: Consolidated 1-D Vibronic Sweep Data for the S_xO_y Candidate Pool, S_2Cl_2.

Author Contributions: P.P. and P.M.—conceptualization, calculations, manuscript text and prepared figures and tables; P.P. and P.M.—writing—original draft preparation; P.M., R.S., M.Y., A.A. and S.—review and editing; A.M., P.T. and A.S.—resources, software, supervision, validation and visualization. All authors have read and agreed to the published version of the manuscript.

Funding: The financial support to Dr. Alka Misra from the Council of Science & Technology (CST) under a major research project (CST/D-2817) and minor research projects under the Research & Devel-

opment Scheme, Department of Higher Education, Government of Uttar Pradesh, (41/2024/336/70-4-2024-001-4(59)/2022) is gratefully acknowledged.

Data Availability Statement: The original contributions presented in this study are included in the article. Further inquiries can be directed to the corresponding authors.

Conflicts of Interest: The authors declare no conflicts of interest. The funders had no role in the design of the study; in the collection, analyses, or interpretation of data; in the writing of the manuscript; or in the decision to publish the results.

References

1. Molaverdikhani, K.; McGouldrick, K.; Esposito, L.W. The Abundance and Vertical Distribution of the Unknown Ultraviolet Absorber in the Venusian Atmosphere from Analysis of Venus Monitoring Camera Images. *Icarus* **2012**, *217*, 648–660. [CrossRef]
2. Bullock, M.A.; Grinspoon, D.H. The Atmosphere and Climate of Venus. *Comp. Climatol. Terr. Planets* **2013**, *1*, 19–54.
3. Pérez-Hoyos, S.; Sánchez-Lavega, A.; García-Muñoz, A.; Irwin, P.G.; Peralta, J.; Holsclaw, G.; McClintock, W.; Sanz-Requena, J.F. Venus Upper Clouds and the UV Absorber from MESSENGER/MASCS Observations. *J. Geophys. Res. Planets* **2018**, *123*, 145–162. [CrossRef]
4. Esposito, L.W.; Knollenberg, R.G.; Marov, M.I.; Toon, O.B.; Turco, R.P. The Clouds and Hazes of Venus. In *Venus*; University of Arizona Press: Tucson, AZ, USA, 1983; pp. 484–564.
5. Svedhem, H.; Titov, D.V.; Taylor, F.W.; Witasse, O. Venus as a More Earth-like Planet. *Nature* **2007**, *450*, 629–632. [CrossRef]
6. Peralta, J.; Lee, Y.J.; McGouldrick, K.; Sagawa, H.; Sánchez-Lavega, A.; Imamura, T.; Widemann, T.; Nakamura, M. Overview of Useful Spectral Regions for Venus: An Update to Encourage Observations Complementary to the Akatsuki Mission. *Icarus* **2017**, *288*, 235–239. [CrossRef]
7. Nakamura, M.; Imamura, T.; Ishii, N.; Abe, T.; Satoh, T.; Suzuki, M.; Ueno, M.; Yamazaki, A.; Iwagami, N.; Watanabe, S.; et al. Overview of Venus Orbiter, Akatsuki. *Earth Planets Space* **2011**, *63*, 443–457. [CrossRef]
8. Glaze, L.S.; Wilson, C.F.; Zasova, L.V.; Nakamura, M.; Limaye, S. Future of Venus Research and Exploration. *Space Sci. Rev.* **2018**, *214*, 89. [CrossRef]
9. Barker, E.S. Detection of SO_2 in the UV Spectrum of Venus. *Geophys. Res. Lett.* **1979**, *6*, 117–120. [CrossRef]
10. Zolotov, M. Sulfur on Venus: Atmospheric, Surface, and Interior Processes. In *The Role of Sulfur in Planetary Processes*; Harlov, D.E., Pokrovski, G.S., Eds.; Springer: Cham, Switzerland, 2026.
11. Frandsen, B.N.; Wennberg, P.O.; Kjaergaard, H.G. Identification of OSSO as a near-UV Absorber in the Venusian Atmosphere. *Geophys. Res. Lett.* **2016**, *43*, 11–146. [CrossRef]
12. Mills, F.; Marcq, E.; Yung, Y.; Parkinson, C.; Jessup, K.L.; Vandaele, A.C. Atmospheric Chemistry on Venus: An Overview of Unresolved Issues. In Proceedings of the 50th Lunar and Planetary Science Conference, The Woodlands, TX, USA, 18–22 March 2019; p. LPI-Contribution No. 2132.
13. Yung, Y.L.; Demore, W.B. Photochemistry of the Stratosphere of Venus: Implications for Atmospheric Evolution. *Icarus* **1982**, *51*, 199–247. [CrossRef]
14. Marcq, E.; Mills, F.P.; Parkinson, C.D.; Vandaele, A.C. Composition and Chemistry of the Neutral Atmosphere of Venus. *Space Sci. Rev.* **2018**, *214*, 10. [CrossRef]
15. Mills, F.; Esposito, L.W.; Yung, Y.L. *Atmospheric Composition, Chemistry, and Clouds. Exploring Venus as a Terrestrial Planet*; The American Geophysical Union: Washington, DC, USA, 2007.
16. Titov, D.V.; Ignatiev, N.I.; McGouldrick, K.; Wilquet, V.; Wilson, C.F. Clouds and Hazes of Venus. *Space Sci. Rev.* **2018**, *214*, 126. [CrossRef]
17. Egan, J.V.; James, A.D.; Plane, J.M. Laboratory Measurements of Ferric Chloride (FeCl3) under Venusian Conditions. *ACS Earth Space Chem.* **2025**, *9*, 2127–2136. [CrossRef]
18. Bierson, C.; Zhang, X. Chemical Cycling in the Venusian Atmosphere: A Full Photochemical Model from the Surface to 110 Km. *J. Geophys. Res. Planets* **2020**, *125*, e2019JE006159. [CrossRef]
19. Dreuw, A.; Head-Gordon, M. Single-Reference Ab Initio Methods for the Calculation of Excited States of Large Molecules. *Chem. Rev.* **2005**, *105*, 4009–4037. [CrossRef]
20. Laurent, A.D.; Jacquemin, D. TD-DFT Benchmarks: A Review. *Int. J. Quantum Chem.* **2013**, *113*, 2019–2039. [CrossRef]
21. Francés-Monerris, A.; Carmona-García, J.; Trabelsi, T.; Saiz-Lopez, A.; Lyons, J.R.; Francisco, J.S.; Roca-Sanjuán, D. Photochemical and Thermochemical Pathways to S2 and Polysulfur Formation in the Atmosphere of Venus. *Nat. Commun.* **2022**, *13*, 4425. [CrossRef] [PubMed]
22. Jiang, C.Z.; Rimmer, P.B.; Lozano, G.G.; Tosca, N.J.; Kufner, C.L.; Sasselov, D.D.; Thompson, S.J. Iron-Sulfur Chemistry Can Explain the Ultraviolet Absorber in the Clouds of Venus. *Sci. Adv.* **2024**, *10*, eadg8826. [CrossRef]

23. Krasnopolsky, V.A. Chemical Composition of Venus Atmosphere and Clouds: Some Unsolved Problems. *Planet. Space Sci.* **2006**, *54*, 1352–1359. [CrossRef]
24. Peach, M.J.; Benfield, P.; Helgaker, T.; Tozer, D.J. Excitation Energies in Density Functional Theory: An Evaluation and a Diagnostic Test. *J. Chem. Phys.* **2008**, *128*, 044118. [CrossRef]
25. Yanai, T.; Tew, D.P.; Handy, N.C. A New Hybrid Exchange–Correlation Functional Using the Coulomb-Attenuating Method (CAM-B3LYP). *Chem. Phys. Lett.* **2004**, *393*, 51–57. [CrossRef]
26. Marenich, A.V.; Cramer, C.J.; Truhlar, D.G. Universal Solvation Model Based on Solute Electron Density and on a Continuum Model of the Solvent Defined by the Bulk Dielectric Constant and Atomic Surface Tensions. *J. Phys. Chem. B* **2009**, *113*, 6378–6396. [CrossRef] [PubMed]
27. Titov, D.V.; Bullock, M.A.; Crisp, D.; Renno, N.O.; Taylor, F.W.; Zasova, L.V. Radiation in the Atmosphere of Venus. *Geophys. Monogr. Am. Geophys. Union* **2007**, *176*, 121.
28. Frisch, M.; Trucks, G.; Schlegel, H.; Scuseria, G.; Robb, M.; Cheeseman, J.; Scalmani, G.; Barone, V.; Petersson, G.; Nakatsuji, H.; et al. *Gaussian 16, Revision A.03*; Gaussian, Inc.: Wallingford, CT, USA, 2016. Available online: https://gaussian.com/relnotes_a03/ (accessed on 18 May 2026).
29. Frisch, M.; Trucks, G.; Schlegel, H.; Scuseria, G.; Robb, M.; Cheeseman, J.; Scalmani, G.; Barone, V.; Petersson, G.; Nakatsuji, H.; et al. *Gaussian 16*; Gaussian, Inc.: Wallingford, CT, USA, 2016. Available online: https://gaussian.com/gaussian16/ (accessed on 18 May 2026).
30. Dennington, R.; Keith, T.A.; Millam, J.M. *GaussView, Version 6.0. 16.*; Semichem Inc.: Shawnee Mission, KS, USA, 2016; pp. 143–150.
31. Basilevsky, A.T.; Head, J.W. The Surface of Venus. *Rep. Prog. Phys.* **2003**, *66*, 1699–1734. [CrossRef]
32. Zhao, Y.; Truhlar, D.G. The M06 Suite of Density Functionals for Main Group Thermochemistry, Thermochemical Kinetics, Noncovalent Interactions, Excited States, and Transition Elements: Two New Functionals and Systematic Testing of Four M06-Class Functionals and 12 Other Functionals. *Theor. Chem. Acc.* **2008**, *120*, 215–241.
33. Zhao, Y.; Truhlar, D.G. Density Functionals with Broad Applicability in Chemistry. *Acc. Chem. Res.* **2008**, *41*, 157–167. [CrossRef] [PubMed]
34. Walker, M.; Harvey, A.J.; Sen, A.; Dessent, C.E. Performance of M06, M06-2X, and M06-HF Density Functionals for Conformationally Flexible Anionic Clusters: M06 Functionals Perform Better than B3LYP for a Model System with Dispersion and Ionic Hydrogen-Bonding Interactions. *J. Phys. Chem. A* **2013**, *117*, 12590–12600. [CrossRef]
35. Weigend, F.; Furche, F.; Ahlrichs, R. Gaussian Basis Sets of Quadruple Zeta Valence Quality for Atoms H–Kr. *J. Chem. Phys.* **2003**, *119*, 12753–12762. [CrossRef]
36. Weigend, F. Accurate Coulomb-Fitting Basis Sets for H to Rn. *Phys. Chem. Chem. Phys.* **2006**, *8*, 1057–1065. [CrossRef]
37. Runge, E.; Gross, E.K. Density-Functional Theory for Time-Dependent Systems. *Phys. Rev. Lett.* **1984**, *52*, 997. [CrossRef]
38. Tawada, Y.; Tsuneda, T.; Yanagisawa, S.; Yanai, T.; Hirao, K. A Long-Range-Corrected Time-Dependent Density Functional Theory. *J. Chem. Phys.* **2004**, *120*, 8425–8433. [CrossRef]
39. Dreuw, A.; Head-Gordon, M. Failure of Time-Dependent Density Functional Theory for Long-Range Charge-Transfer Excited States: The Zincbacteriochlorin−Bacteriochlorin and Bacteriochlorophyll−Spheroidene Complexes. *J. Am. Chem. Soc.* **2004**, *126*, 4007–4016. [CrossRef] [PubMed]
40. Peach, M.J.G.; Helgaker, T.; Sałek, P.; Keal, T.W.; Lutnæs, O.B.; Tozer, D.J.; Handy, N.C. Assessment of a Coulomb-Attenuated Exchange–Correlation Energy Functional. *Phys. Chem. Chem. Phys.* **2006**, *8*, 558–562. [CrossRef]
41. Jacquemin, D.; Perpète, E.A.; Scuseria, G.E.; Ciofini, I.; Adamo, C. TD-DFT Performance for the Visible Absorption Spectra of Organic Dyes: Conventional versus Long-Range Hybrids. *J. Chem. Theory Comput.* **2008**, *4*, 123–135. [CrossRef]
42. Zasova, L.V.; Ignatiev, N.; Khatuntsev, I.; Linkin, V. Structure of the Venus Atmosphere. *Planet. Space Sci.* **2007**, *55*, 1712–1728. [CrossRef]
43. Tomasi, J.; Mennucci, B.; Cammi, R. Quantum Mechanical Continuum Solvation Models. *Chem. Rev.* **2005**, *105*, 2999–3094. [CrossRef]
44. Reichardt, C. Solvatochromic Dyes as Solvent Polarity Indicators. *Chem. Rev.* **1994**, *94*, 2319–2358. [CrossRef]
45. Cobos, C.J.; Croce, A.E. Theoretical Study of the Electronic Spectrum of Disulfur Monoxide. *Z. Naturforschung A* **2014**, *69*, 215–219. [CrossRef]
46. Trabelsi, T. Spectroscopic Characterization of S_3 O Isomers: Potential Contributor to the Unknown UV Absorber in Venus's Atmosphere. *J. Phys. Chem. A* **2025**, *129*, 4870–4878. [CrossRef]
47. Trabelsi, T.; Francico, J.S. Chlorine–Sulfur Isomers as Parents of ClS_2 and SCl_2 on Venus: Spectroscopy and Photochemistry of ClSSCl, $SSCl_2$, and $(ClS)_2$. *J. Chem. Phys.* **2026**, *164*, 084302. [CrossRef]
48. Lee, S.-Y. Energy Shift Correction for the Reflection Approximation. *J. Chem. Phys.* **1985**, *82*, 4588–4594. [CrossRef]
49. Sršeň, Š.; Slavíček, P. Optimal Representation of the Nuclear Ensemble: Application to Electronic Spectroscopy. *J. Chem. Theory Comput.* **2021**, *17*, 6395–6404. [CrossRef] [PubMed]

50. Jank, D.; Ončák, M.; Jin, S.; Van Der Linde, C.; Beyer, M.K. Multiconfigurational Character of Repulsive $A^2\,\Sigma_g^+$ State Leaves Strong Signature in the Photodissociation Spectrum of Zn_2^+. *J. Am. Chem. Soc.* **2024**, *146*, 16385–16388. [CrossRef] [PubMed]
51. Jessup, K.L.; Marcq, E.; Mills, F.; Mahieux, A.; Limaye, S.; Wilson, C.; Allen, M.; Bertaux, J.-L.; Markiewicz, W.; Roman, T.; et al. Coordinated Hubble Space Telescope and Venus Express Observations of Venus' Upper Cloud Deck. *Icarus* **2015**, *258*, 309–336. [CrossRef]
52. Bains, W.; Petkowski, J.J.; Seager, S.; Ranjan, S.; Sousa-Silva, C.; Rimmer, P.B.; Zhan, Z.; Greaves, J.S.; Richards, A.M.S. Phosphine on Venus Cannot Be Explained by Conventional Processes. *Astrobiology* **2021**, *21*, 1277–1304. [CrossRef] [PubMed]
53. Greaves, J.S.; Richards, A.M.S.; Bains, W.; Rimmer, P.B.; Clements, D.L.; Seager, S.; Petkowski, J.J.; Sousa-Silva, C.; Ranjan, S.; Fraser, H.J. Re-Analysis of Phosphine in Venus' Clouds. *Nat. Astron.* **2021**, *5*, 636–639. [CrossRef]
54. Bertaux, J.; Widemann, T.; Hauchecorne, A.; Moroz, V.I.; Ekonomov, A.P. VEGA 1 and VEGA 2 Entry Probes: An Investigation of Local UV Absorption (220–400 Nm) in the Atmosphere of Venus (SO_2 Aerosols, Cloud Structure). *J. Geophys. Res.* **1996**, *101*, 12709–12745. [CrossRef]
55. Zhang, X.; Liang, M.C.; Mills, F.P.; Belyaev, D.A.; Yung, Y.L. Sulfur Chemistry in the Middle Atmosphere of Venus. *Icarus* **2012**, *217*, 714–739. [CrossRef]
56. Sánchez-Lavega, A.; Lebonnois, S.; Imamura, T.; Read, P.; Luz, D. The Atmospheric Dynamics of Venus. *Space Sci. Rev.* **2017**, *212*, 1541–1616. [CrossRef]
57. Krasnopolsky, V.A. A Photochemical Model for the Venus Atmosphere at 47–112km. *Icarus* **2012**, *218*, 230–246. [CrossRef]
58. Krasnopolsky, V.A. S3 and S4 Abundances and Improved Chemical Kinetic Model for the Lower Atmosphere of Venus. *Icarus* **2013**, *225*, 570–580. [CrossRef]